energies

MDPI

Review

Experimental Investigations and Numerical Studies of Two-Phase Countercurrent Flow Limitation in a Pressurized Water Reactor: A Review

Xixi Zhu [1], Zhengguang Wang [2], Chende Xu [2] and Naihua Wang [1,*]

[1] Institute of Thermal Science and Technology, Shandong University, Jinan 250061, China
[2] State Key Laboratory of Nuclear Power Safety Monitoring Technology and Equipment, China Nuclear Power Engineering Co., Ltd., Shenzhen 518172, China
* Correspondence: wnh@sdu.edu.cn

Abstract: Gas–liquid two-phase countercurrent flow limitation (CCFL) phenomena widely exist in nuclear power plants. In particular, the gas–liquid countercurrent flow limitation phenomena in a pressurized water reactor (PWR) during a loss-of-coolant accident (LOCA) or a small-break loss-of-coolant accident (SBLOCA) play an important role in nuclear reactor safety research. Over several decades, a series of experimental investigations and numerical studies have been carried out to study the CCFL phenomena in a PWR. For the experimental investigations, numerous experiments have been conducted, and different CCFL mechanisms and CCFL characteristics have been obtained in various test facilities simulating different scenarios in a PWR. The CCFL phenomena are affected by many factors, such as geometrical characteristics, liquid flow rates, and fluid properties. For the numerical studies, more and more numerical models were presented and applied to the calculations of two-phase countercurrent flow over the past several decades. It is considered that the computational fluid dynamics (CFD) tools can simulate most of the two-phase flow configurations encountered in nuclear power plants. In this paper, the experimental investigations and the numerical studies on two-phase countercurrent flow limitation in a PWR are comprehensively reviewed. This review provides a further understanding of CCFL in a PWR and gives directions regarding future studies. It is found that relatively fewer investigations using steam–water under high system pressures are performed due to the limitation of the test facilities and test conditions. There are a number of numerical studies on countercurrent two-phase flow in a PWR hot leg geometry, but the simulations in other flow channels were relatively rare. In addition, almost all of the numerical simulations do not include heat and mass transfer. Thus, it is necessary to investigate the effects of heat and mass transfer experimentally and numerically. Furthermore, it is of significance to perform numerical simulations for countercurrent two-phase flow with a fine computational grid and suitable models to predict the formation of small waves and the details in two-phase flow.

Keywords: CCFL; PWR; two-phase flow; countercurrent; flooding; hot leg; surge line; obstruction; review

Citation: Zhu, X.; Wang, Z.; Xu, C.; Wang, N. Experimental Investigations and Numerical Studies of Two-Phase Countercurrent Flow Limitation in a Pressurized Water Reactor: A Review. *Energies* **2023**, *16*, 1487. https://doi.org/10.3390/en16031487

Academic Editor: Li Chen

Received: 28 December 2022
Revised: 24 January 2023
Accepted: 30 January 2023
Published: 2 February 2023

1. Introduction

Gas–liquid two-phase countercurrent flow widely exists in practical applications of industrial systems such as nuclear reactors, steam generation, oil and gas pipelines and refrigeration equipment, reflux condensers, packed columns, heat pipes, etc. In particular, gas–liquid countercurrent flow can be seen frequently during various transient phases in a pressurized water reactor (PWR), and the countercurrent flow limitation phenomena play an important role in reactor safety due to their influence on the thermohydraulic behavior of PWRs during a loss-of-coolant accident (LOCA) or a small-break loss-of-coolant accident (SBLOCA). The flow is called countercurrent flow (CCF) when the gas and liquid are flowing in opposite directions. For a certain range of gas and liquid flow rates, the CCF is a stratified flow, and the downflowing liquid flow rate is equal to the inlet liquid flow rate.

There exists a maximum gas flow rate at which the downflowing liquid flow rate is equal to the inlet water flow rate with the gradual increase of the gas flow rate [1]. This limiting condition is called countercurrent flow limitation (CCFL), which is also known as the onset of flooding.

In a PWR, the emergency core coolant system (ECCS) injects cold water during the blowdown phase of a big-break accident to lower the temperature of the fuel elements, which rises quickly as a result of the radioactive decay of the fission products. The steam flow in the opposite direction at some crucial locations, such as at the reactor vessel downcomer, the upper tie plate, and in the U-tubes of the steam generator, might limit the penetration of the cold water in the PWR primary circuit. In the scenario of a SBLOCA, depressurization and vaporization will generate steam on the primary side. The steam condenses in the U-tubes of the steam generator, and the condensed water falls through the hot leg. This situation corresponds to "reflux condensation" [2,3]. The blowdown valves on the pressurizer of the first to third stages of the automatic depressurization system (ADS 1–3) and the valves of the fourth stage of the automatic depressurization system (ADS 4) will be opened during a SBLOCA, and then the water in the pressurizer flows downward along the pressurizer surge line driven by the gravity, thus forming a steam-water countercurrent flow in the surge line [4]. CCFL phenomena may occur in all these scenarios, and the prediction of CCFL becomes important for the analysis of nuclear safety.

A large number of researchers have carried out experimental and theoretical studies of two-phase countercurrent flow to explore the CCFL mechanism and CCFL characteristics over the last several decades. The earliest work was performed by Wallis [5], which turned into a reference for many other researchers. Extensive relevant experiments have been conducted in the vertical channel, horizontal channel, inclined channel, PWR hot leg, and pressurizer surge line.

Bankoff and Lee [6] reviewed the adiabatic two-phase flow and condensing two-phase flow in vertical and inclined channels. They classified the analytical flooding models as envelope theory, traveling wave stability theory, static equilibrium theory, and slug formation theory. They also indicated that more studies should be performed to study the various parametric effects, including the tube length effect, the condensing effect, and the condensation-induced water hammer.

Some researchers reviewed the related literature on the CCFL phenomenon in a PWR hot leg during a LOCA or a SBLOCA [7–9]. Issa and Macian [7] presented the previous experimental studies on the CCFL phenomenon and the different factors that govern CCFL in a PWR hot leg. They reviewed the affecting parameters of CCFL, such as the liquid superficial velocity, the geometrical characteristics, the physical properties, and so on. They collected and grouped the available CCFL data and CCFL correlations to establish a data bank of CCFL. They indicated that many geometrical and scaling effects are currently unclear. Deendarlianto et al. [8] performed a research review of the experimental investigations and the analytical studies on gas–liquid CCFL in a PWR hot leg. They proposed that many applied correlations are observed under a narrow range of conditions and are restricted to the specific test geometry and test conditions. They found that the physical mechanisms of CCFL occurrence are still not fully understood, and some researchers obtained contradictory conclusions on flooding mechanisms, despite the fact that the experiments were performed under identical conditions. They recommended that the advanced experimental procedure and apparatus, and new flow measurement techniques with advanced image processing, are required to obtain highly reliable experimental data and to explain the flooding mechanisms in the future. A brief review of the computational fluid dynamics (CFD) application of the CCFL phenomenon is also presented. Deendarlianto et al. suggested that the relevant literature is rare and more CFD studies regarding CCFL are needed. Morghi et al. [9] review the recent experimental investigations of CCFL for different geometries of hot leg in a PWR. They compared the recent experimental results with those of Navarro [2] and found these results are in good agreement.

It can be seen that the existing review articles are all overviews of CCFL for specific geometries, such as vertical or inclined channels and PWR hot legs. There is no comprehensive and systematic CCFL review that covers various geometrical channels, including the vertical channel, horizontal channel, inclined channel, PWR hot leg and surge line, etc., used for different scenarios in a PWR. Computational fluid dynamics has developed rapidly in recent years, and the numerical studies of CCFL in a PWR using CFD have become a new interest in nuclear reactor safety research. It is necessary to review the relevant numerical studies on the CCFL phenomenon in a PWR, which is beneficial to understand the CCFL mechanisms and CCFL characteristics.

The objective of our paper is to summarize the previous investigations of the two-phase CCFL in a PWR, experimentally and numerically. In this paper, we perform a comprehensive overview of the recent experimental investigations of CCFL in various geometrical channels firstly. The experimental investigations are classified by the geometry of the flow channel. The CCFL characteristics, void friction, pressure drop, liquid film, flow pattern, and the gas–liquid interface characteristics are discussed, and the CCFL correlations proposed by different researchers are concluded in this part. In the next part, CFD-based numerical studies of CCFL in a PWR are summarized. Finally, the conclusions are made, and the directions of future research in this area are presented.

2. Fundamentals of CCFL

In this section, the fundamentals of CCFL are introduced, including the basic definitions of CCF and major parameters related to CCFL.

In gas–liquid two-phase flow, if the gas and liquid are flowing in opposite directions, the flow is called CCF, as shown in Figure 1. For a certain range of gas and liquid flow rates, the CCF is a stratified flow, and the downflowing liquid flow rate is equal to the inlet liquid flow rate. There exists a maximum gas flow rate at which the downflowing liquid flow rate is equal to the inlet water flow rate with the gradual increase of the gas flow rate. This limiting condition is called CCFL. In the study of Celata et al. [10], the onset of flooding was defined as the condition at which the liquid falling film starts to be entrained by the upward-flowing gas. Actually, the CCFL refers to the onset of flooding in most literature.

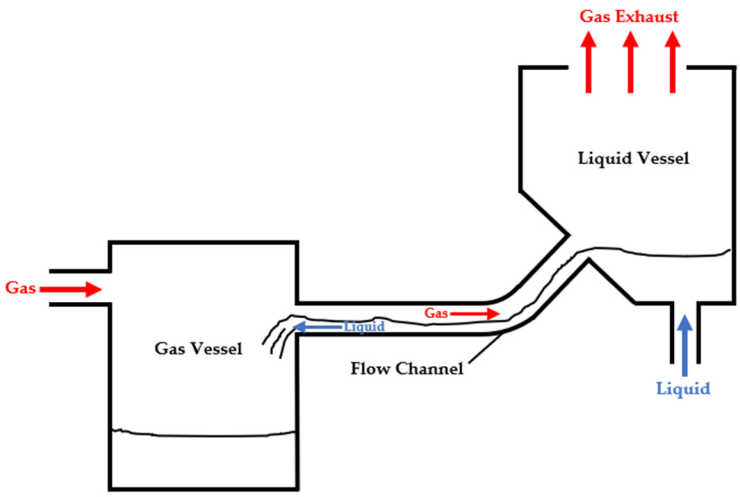

Figure 1. Schematic diagram of CCF.

Kang et al. [11] divided the whole development process of CCFL into three categories: the onset of flooding, the partial liquid delivery, and the zero liquid penetration (ZP), as Figure 2 shows. The zero liquid penetration corresponds to the point at which the falling water flow rate is close to zero, and the region between the CCFL and ZP is defined as the partial delivery region. Note that the development process of CCFL above was obtained by setting the liquid flow rate as a specified value and gradually increasing the gas flow

rate. In turn, when the gas flow rate decreases, there comes the point at which a fully countercurrent two-phase flow is established. This is known as the deflooding point.

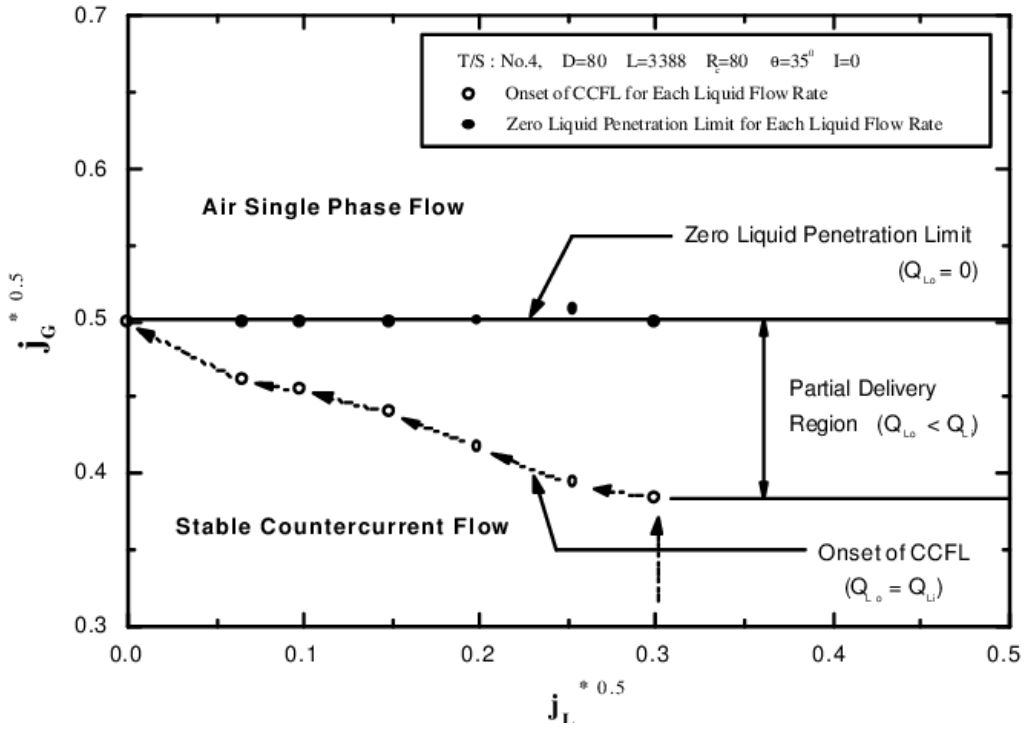

Figure 2. The typical CCFL curve obtained with a hot leg model by using Wallis parameters (Kang et al. [11]).

Many researchers observed a sudden change of the two-phase flow pressure drop in the test section at the onset of flooding and deflooding. The pressure drop increases slightly until the onset of flooding is reached, then the pressure drop starts to increase suddenly duo to the flow instability. Additionally, the pressure drop decreases suddenly at the deflooding point. In some experimental investigations, a hysteresis phenomenon between the onset of flooding and deflooding was observed. The hysteresis phenomenon corresponds to the gas flow rate needed for the onset of flooding being greater than that necessary for the occurrence of deflooding. Note that the "CCFL data" term was used in most literature. It is necessary to carefully distinguish the processes of flooding, deflooding, and partial delivery when referring to CCFL data.

The accurate prediction of the CCFL occurrence is important for nuclear reactor safety. A series of empirical correlations based on the related dimensionless parameters have been proposed by different researchers to predict the occurrence of CCFL. The two most widely used dimensionless parameters are the Wallis parameter and Kutateladze number.

Wallis [5] proposed the dimensionless parameter, J_K^*, which represents the ratio between inertial force and hydrostatic force, and is defined as follows:

$$J_K^* = J_K \sqrt{\frac{\rho_K}{(\rho_L - \rho_G) g D}} \tag{1}$$

Note that J_K is the gas/liquid superficial velocity instead of the actual velocity.

Another dimensionless parameter that is frequently used is the Kutateladze number, Ku_K^*, and is defined as:

$$Ku_K^* = \frac{J_K \rho_K^{1/2}}{[(\rho_L - \rho_G) g \sigma]^{1/4}} \tag{2}$$

The Wallis parameter and Kutateladze number are similar, and the relationship between these two dimensionless parameters can be described as follows,

$$Ku_K^* = J_K^*(D^*)^{1/2} \tag{3}$$

where D^* is the dimensionless hydraulic diameter, and is defined as,

$$D^* = D\sqrt{\frac{(\rho_L - \rho_G)g}{\sigma}} \tag{4}$$

It is worth noting that the Wallis parameter and Kutateladze number were obtained originally based on the countercurrent flow in vertical pipes. Since then, they were applied to other geometrical channels, such as horizontal pipes and PWR hot legs, and satisfactory results were obtained. It is reported that the Wallis parameter and the Kutateladze number are applicable for small inner pipe diameters and large ones, respectively [12].

3. Experimental Investigations

In this section, a review of the experimental investigations on the CCFL in a PWR is performed. Large numbers of experimental works were carried out to study the CCFL mechanisms, the CCFL characteristics, and the affecting factors of CCFL in various flow channels. The CCFL is strongly affected by the geometry of the test flow channel. In terms of the flow channel geometry, the experimental investigations are divided into several categories: those studying the vertical channel, horizontal and nearly horizontal channel, inclined channel, flow channel with elbow, and flow channel with obstruction.

3.1. Vertical Channel

Table 1 summarizes of the previous experimental investigations on the CCFL in vertical channels. It can be seen that the earliest experimental investigation on CCFL in a vertical channel was carried out by Wallis [5]. Wallis performed the air–water countercurrent flow experiment in a vertical pipe and proposed the most frequently used empirical correlation known as the Wallis-type correlation. Soon afterward, numerous CCFL experimental studies were performed in vertical channels at various test facilities.

The Wallis-type correlation can be described as:

$$J_G^{*1/2} + mJ_L^{*1/2} = C \tag{5}$$

where m and C are both constants determined from experiments, $m = 0.8 \sim 1.0$ and $C = 0.7 \sim 1.0$.

Another empirical correlation that is frequently used is expressed in terms of the Kutateladze number:

$$Ku_G^{*1/2} + mKu_L^{*1/2} = C \tag{6}$$

Pushkina and Sorokin [13] gave $m = 0$, $C = 1.79$. They proposed that the Wallis-type correlation is not substantiated by empirical data. They also reported that the inner pipe diameter has practically no effect on the critical velocity with respect to the reversal of the motion of the liquid film. Chung et al. [14] reported that $0.65 \leq m \leq 0.8$ and C is a function of the dimensionless diameter D^*. They proposed that flooding is strongly influenced by flow channel geometry and liquid physical properties.

Table 1. Summary of the experimental investigations on the CCFL in vertical channels.

Authors	Test Fluids	Inner Pipe Diameter (mm)	Pipe Length (m)	Empirical Correlation	Remarks
Wallis [5] (1961)	Air–water	-	-	$J_G^{*1/2} + mJ_L^{*1/2} = C$ $m = 0.8 \sim 1.0$, $C = 0.7 \sim 1.0$	The empirical correlation was obtained in the vertical countercurrent two-phase flow
Pushkina and Sorokin [13] (1969)	Air–water	12, 31, 310	2.5	$Ku_G^{*1/2} + mKu_L^{*1/2} = C$ $m = 0$, $C = 1.79$	The Wallis-type correlation is not substantiated by empirical data
Chung et al. [14] (1980)	Air–water, air–silicone oil, air–white oil	15.9, 31.8, 46, 70	0.914	$Ku_G^{*1/2} + mKu_L^{*1/2} = C = C_1 \tanh\left(C_2 D^{*1/4}\right)$ $m = 0.65 \sim 0.8$, $C_1 = 1.79 \sim 2.1$, $C_2 = 0.8 \sim 0.9$	Flooding is strongly influenced by flow channel geometry and liquid physical properties.
Mcquillan et al. [15] (1985)	Air–water	32	1.0	-	The occurrence of flooding is a result of the formation and movement of a large disturbance wave
Suzuki and Ueda [16] (1977)	Air–water, air–aqueous glycerol solution, air–aqueous sec-octyl alcohol solution	10, 18, 28.8	0.5, 1.0, 1.5, 2.0	-	The effects of the pipe diameter, pipe length, and surface tension were investigated
Osakabe and Kawasaki [17] (1989)	Air–water	Width × Gap for rectangular channel: 100 × 10, 100 × 5, 100 × 2	1.235	$J_G^{*1/2} + 0.8J_L^{*1/2} = 0.58$	The channel width strongly affects the flooding velocity The correlated CCFL correlation employs the channel width as the characteristic length
Sudo et al. [18] (1991)	Air–water	Inner diameter for circular channel: 8, 12, 20 Width × Gap for rectangular channel: 66 × 2.3; 66 × 5.3; 66 × 8.3; 66 × 12.3; 33 × 2.3; 33 × 5.3; 33 × 8.3; 33 × 12.3	0.25, 0.75 (circular channel length) 0.072, 0.362, 0.782 (rectangular channel length)	$Y = 1.3e^{-2.1X}$ $X = \left(\frac{m}{C}\right) j_{Lb}^{*1/2}$, $Y = \left(\frac{1}{C}\right) j_{Gb}^{*1/2}$	The channel gap was selected as the characteristic length The flooding air velocity decreases significantly as the channel gap increases, and the channel length has little influence on the CCFL
Vijayan et al. [19] (2001)	Air–water	25, 67, 99	0.5, 1.8	-	Three distinct flooding mechanisms were observed The flooding mechanisms are different in small and large diameter pipes
Drosos et al. [20] (2006)	Air–water, air–1.5% butanol solution, air–2.5% butanol solution,	Rectangular channel gap: 10	0.38	-	The effect of the fluid property was investigated The flooding velocity significantly increases as the interfacial tension increases
Matsumura and Kaminaga [21] (2012)	Air–water	12, 20	1.0	For the 20 mm diameter pipe, $J_G^{*1/2} + 0.9J_L^{*1/2} = 0.78$ For the 20 mm diameter pipe, $J_G^{*1/2} + mJ_L^{*1/2} = 1$ ($m = 1.8$ when $h = 0.05$, 0.1 m; $m = 2.0$ when $h = 0.2$ m)	The water level in the upper plenum affects the CCFL characteristics in the 12 mm diameter pipe but does not in the 20 mm diameter pipe
Doi et al. [22] (2012)	Air–water	30, 45, 60	10D	-	The upper tank geometry and upper tank water level have effects on CCFL
Kusunoki et al. [23] (2015)	Air–40 wt% glycerol water solution, air–60 wt% glycerol water solution, saturated steam–water	14, 20, 27	0.5	$\frac{J_G^{*1/2}}{(\mu_G/\mu_L)^{0.07}} = (1.04 \pm 0.05) - 3.6\left[\left(\frac{\mu_G}{\mu_L}\right)^{0.1} (J_L^*)^{1/2}\right] + 11\left[\left(\frac{\mu_G}{\mu_L}\right)^{0.1} (J_L^*)^{1/2}\right]^2 - 16\left[\left(\frac{\mu_G}{\mu_L}\right)^{0.1} (J_L^*)^{1/2}\right]^3$	The flooding gas velocity decreases as the liquid viscosity increases The pipe diameter has little effect on CCFL characteristics through steam-water experiments The viscosity ratio is more suitable to predict the CCFL compared with the dimensionless inverse viscosity
Wan et al. [24] (2021)	Air–water	25	1.8	-	The liquid film thickness was measured by employing a parallel electrode probe Two flooding mechanisms were observed
Ma et al. [25] (2023)	Air–water	12–100	0.5–2.0	$Ku_G^{0.5}\mu_G^{*0.1} + m_1 Ku_L^{0.5}\mu_L^{*0.1} - m_2\left(Ku_L^{0.5}\mu_L^{*0.1}\right)^2 = 0.49$ $m_1 = -0.36 \times 10^{-2}\left(\frac{L}{D}\right)^2 + 0.12\frac{L}{D} + 1.11$, $m_2 = -1.23 \times 10^{-2}\left(\frac{L}{D}\right)^2 + 0.39\frac{L}{D} + 0.18$	The flooding velocity increases with increasing the pipe diameter A novel empirical correlation of CCFL was developed

Mcquillan et al. [15] employed an axial view photographic technique to observe the flow information, which is important for the investigations of the flooding mechanisms. They observed that the onset of flooding is a result of the formation of a wavelike disturbance and of the subsequent upward movement of the large disturbance wave along the pipe. Before the formation of the flooding disturbance, there was almost no water droplet entrainment and no upward movement of the droplets. The droplets were entrained from the tip of the flooding disturbance and traveled up along the pipe.

In order to explore the CCFL mechanism in a vertical pipe, Wan et al. [24] carried out air–water countercurrent flow experiments. A parallel electrode probe was employed to obtain the liquid film behavior characteristics. In the experiments, two flooding mechanisms were observed. At low water flow rates, the occurrence of CCFL is a result of the upward propagation of interfacial waves. At high water flow rates, the liquid bridging in the pipe, which occurs due to the turbulent flow pattern, directly leads to the occurrence of CCFL.

They also suggested that there exists a transition region at which the two CCFL mechanisms all take place.

Besides the investigations of flooding mechanisms in vertical channels, most researchers studied the various affecting factors of CCFL, including the pipe cross-section geometry, the pipe diameter, the pipe length, the physical properties, and the entrance and exit conditions. Suzuki and Ueda [16] conducted two-phase countercurrent experiments in vertical pipes. An air–water, air–aqueous glycerol solution and air–aqueous sec-octyl alcohol solution were employed as working fluids. They found that the flooding air velocity decreases with the liquid flow rate and the pipe length increase and increases as the pipe diameter increases. The influence of the pipe length on flooding becomes smaller when the liquid viscosity is large. The influence of surface tension is complicated; there exists a surface tension value at which the greatest flooding air velocity is reached. In addition, they revealed the complicated effects of pipe length and surface tension on flooding by the measurements of the maximum height of wavy liquid films. Later, Ueda and Suzuki [26] carried out flooding experiments in annuli and rod bundle channels. They proposed that the experimental data for annuli and rod bundle channels are also well-correlated with the equivalent diameter.

Vijayan et al. [19] experimentally investigated the influence of pipe diameter on the flooding mechanism in a vertical channel. Three different inner pipe diameters were used. Results showed that the flooding mechanisms are qualitatively different in the small-diameter pipe and large-diameter pipes. Three distinct flooding mechanisms were observed: the upward transport of ring-type waves, carryover of liquid in the form of droplets, and carryover of liquid in the form of large waves in churn-like motion. They reported that the first flooding mechanism only occurs in the 25 mm diameter pipe, the second flooding mechanism takes place in the 67 mm and 99 mm diameter pipes at a low water flow rate, and the third one happens at a high water flow rate. They also investigated the effect of pipe length on flooding, but experiments with only two different pipe lengths were carried out, and the influence of pipe length remains to be quantified accurately.

Matsumura and Kaminaga [21] performed air–water countercurrent flow experiments in vertical pipes to investigate the CCFL characteristics and the rising gas bubble characteristics. Results showed that one bubble formation cycle corresponds to one pressure fluctuation cycle. The water level in the upper plenum affects the CCFL characteristics in the 12 mm diameter pipe but does not in the 20 mm diameter pipe. They found that the Wallis-type correlation can well predict the CCFL characteristics in the experiments.

For the 20 mm diameter pipe, the correlation was written as:

$$J_G^{*1/2} + 0.9 J_L^{*1/2} = 0.78 \tag{7}$$

For the 12 mm diameter pipe, the correlation was written as:

$$J_G^{*1/2} + m J_L^{*1/2} = 1 \tag{8}$$

where $m = 1.8$ when the water level in the upper plenum is 0.05 m and 0.1 m, while $m = 2.0$ when the water level is 0.2 m.

Doi et al. [22] performed CCFL experiments in vertical pipes with various upper tank geometries and different tank water levels. They found that not only the pipe geometry but also the tank geometry and the tank water level affected the CCFL characteristics. For the rectangular upper tank, CCFL takes place at the junction between the upper tank and the pipe. For the cylindrical upper tank, CCFL occurs at the junction and inside the test pipe under a high air flow rate in a small diameter pipe. The CCFL is mitigated with the increase of the water level in the cylindrical upper tank and the air volume in the lower tank. They proposed that the CCFL characteristics can be well-correlated by using Kutateladze numbers.

To evaluate the effect of the liquid viscosity on CCFL characteristics, Kusunoki et al. [23] conducted experiments in a vertical pipe. Test fluids in the experiments were air–glycerol water solutions and saturated steam–water. They suggested that it is suitable to employ the Wallis parameters instead of the Kutateladze numbers. The results indicated that the flooding gas velocity decreases with the increase of liquid viscosity. They found that the pipe diameter has little effect on CCFL characteristics through the experiments using steam–water. They also evaluated the effect of the dimensionless inverse viscosity or the viscosity ratio as a correction term. The results showed that the viscosity ratio is more suitable for the correlation terms to predict the CCFL, and a Wallis-type correlation was proposed as below.

$$\begin{aligned}\frac{J_G^{*1/2}}{(\mu_G/\mu_L)^{0.07}} &= (1.04 \pm 0.05) - 3.6\left[\left(\frac{\mu_G}{\mu_L}\right)^{0.1}(J_L^*)^{1/2}\right] \\ &+11\left[\left(\frac{\mu_G}{\mu_L}\right)^{0.1}(J_L^*)^{1/2}\right]^2 - 16\left[\left(\frac{\mu_G}{\mu_L}\right)^{0.1}(J_L^*)^{1/2}\right]^3\end{aligned} \tag{9}$$

To clarify the effects of pipe diameter and pipe length on the CCFL, Ma et al. [25] conducted countercurrent flow experiments in vertical pipes with pipe diameter and pipe length ranges of 25–100 mm and 0.5–2.0 m, respectively. Results indicated that the pipe diameter has a great influence on the CCFL, and the flooding velocity increases with an increasing pipe diameter. A novel empirical correlation of CCFL was developed to reveal the effect of pipe diameter and pipe length, and is described as follows.

$$\begin{aligned}Ku_G^{0.5}\mu_G^{*0.1} + m_1 Ku_L^{0.5}\mu_L^{*0.1} - m_2\left(Ku_L^{0.5}\mu_L^{*0.1}\right)^2 &= 0.49 \\ m_1 = -0.36\times10^{-2}\left(\frac{L}{D}\right)^2 + 0.12\frac{L}{D} + 1.11; \\ m_2 = -1.23\times10^{-2}\left(\frac{L}{D}\right)^2 + 0.39\frac{L}{D} + 0.18\end{aligned} \tag{10}$$

where μ^* characterizes the ratio of viscous force to buoyancy, and is defined as:

$$\mu_G^* = \frac{\mu_G J_G}{D^2 g(\rho_L - \rho_G)} \tag{11}$$

$$\mu_L^* = \frac{\mu_L J_L}{D^2 g(\rho_L - \rho_G)} \tag{12}$$

It can be seen that most CCFL experiments are performed in vertical channels with a circular cross-section. Additionally, some researchers investigated CCFL in rectangular channels [17,18,20]. Osakabe and Kawasaki [17] proposed that the channel width of the thin rectangular channel strongly affects the flooding velocity. They correlated the CCFL characteristic by using the width as the characteristic length in Wallis parameters. On the contrary, Sudo et al. [18] and Drosos et al. [20] selected the channel gap as the characteristic length. Sudo et al. [18] carried out CCFL experiments in vertical channels with both rectangular and circular cross-sections to investigate the CCFL characteristics in the vertical rectangular channel. The experiments all proceeded with a constant water level in the upper plenum. Results indicated that the flooding air velocity decreases significantly as the channel gap increases, and that the channel length has little influence on the CCFL. An empirical correlation made by using new dimensionless parameters based on the Wallis parameter was proposed to predict the CCFL as:

$$Y = 1.3e^{-2.1X} \tag{13}$$

where X and Y are the two new dimensionless parameters, and are defined as:

$$X = \left(\frac{m}{C}\right)J_{Lb}^{*1/2} \tag{14}$$

$$Y = \left(\frac{1}{C}\right) J_{Gb}^{*1/2} \tag{15}$$

where $J_{Lb}^{*1/2}$ and $J_{Gb}^{*1/2}$ are the Wallis parameters by using the channel gap as the characteristic length, m and C are the functions of the channel width a, the channel gap b and the physical properties of the working fluids, and are given as below,

$$m = 0.5 + 0.0015 Bo^{*1.3} \tag{16}$$

$$C = 0.66\left(\frac{b}{a}\right) \tag{17}$$

where the dimensionless parameter Bo^* is defined as:

$$Bo^* = \frac{ab(\rho_L - \rho_G)g}{\sigma} \tag{18}$$

To investigate the influences of fluid properties on CCFL, Drosos et al. [20] conducted experiments in a vertical rectangular channel using air and different liquids. They reported that the flooding velocity significantly increases with the interfacial tension increases. It is worth mentioning that many investigations focusing on the interfacial friction factor were performed experimentally by some researchers [27–32].

3.2. Horizontal and Nearly Horizontal Channels

The flooding phenomenon in the horizontal or nearly horizontal channel is also of great significance in the reactor safety analysis. The experimental studies on CCFL in the horizontal and nearly horizontal channels are listed in Table 2. For the countercurrent two-phase flow in a horizontal or nearly horizontal channel, the criteria for the onset of slug flow and the onset of flooding have been widely investigated. Wallis and Dobson [33] presented a simple criterion for the occurrence of slug or plug flow regime in horizontal rectangular channels. Gardner [34] performed countercurrent two-phase flow experiments and developed the criterion for flooding in horizontal countercurrent flow.

Table 2. Summary of the experimental investigations on the CCFL in horizontal and nearly horizontal channels.

Authors	Test Fluids	Inner Pipe Diameter (mm)	Pipe Length (m)	Inclination Angle (°)	Empirical Correlation	Remarks
Wallis and Dobson [33] (1973)	Air–water	Rectangular channel width: 25.4, 89; rectangular channel height: 25.4, 0.076–0.305	1.52, 0.915–6.4	0	$J_G^{*1/2} = 0.5\alpha^{3/2}$	A simple criterion for the onset of slug or plug flow regime in horizontal rectangular channels was presented
Gardner [34] (1983)	Air–water	72	1.18	-	-	The criterion for flooding in horizontal countercurrent flow was developed
Bankoff and Lee [35] (1987)	Steam–water	Rectangular channel width: 95; rectangular channel height: 95	1.3	4.0	-	The onset of flooding was classified into bottom flooding and top flooding, and the flooding location depends on the water injection rate The hysteresis effects in the steam-water flow were observed
Ansari and Nariai [36] (1989)	Air–water	Rectangular channel width: 50; rectangular channel height: 100	8.16	0	-	Three zones in the whole horizontal channel were observed Two slug formation categories were proposed: slug initiation by short wavelength waves and slug initiation by mixed waves
Wang and Kondo [37] (1990)	Air–water	Rectangular channel width: 35; rectangular channel height: 20, 35, 50	0.5, 1.5	0	-	Three various air–water interface behaviors of CCFL for different liquid friction were observed
Choi and No [38] (1995)	Air–water	40, 60, 70	2.16	0.23, 0.69, 0.92	$J_G^{*1/2} + 0.64 J_L^{*1/2} = 0.58$	Two flooding mechanisms were proposed: inner flooding and entrance flooding The effects of pipe diameter, pipe end geometry, and inclination angle on flooding were studied

Table 2. *Cont.*

Authors	Test Fluids	Inner Pipe Diameter (mm)	Pipe Length (m)	Inclination Angle (°)	Empirical Correlation	Remarks
Chun and Yu [39,40] (1999, 2000)	Air–water, Steam–water	83	2.2	0.25, 0.5	$J_G^{*1/2} + 0.6J_L^{*1/2} = 0.52$	The effect of steam condensation on CCFL was investigated
Gargallo et al. [41] (2005)	Air–water	Rectangular channel width: 110; rectangular channel height: 90	440	0 ± (30 µm/500 mm)	$J_G^{*1/2} + J_L^{*1/2} = C$ $C \geq 0.7$	The flooding velocity was found to be sensitive to the inclination angle
Ma et al. [42] (2020)	Air–water	20, 40, 70, 100, 130	2.0	0	For $D \geq 100$ mm, $J_G^{*1/2} + 0.388J_L^{*1/2} + 0.49J_L^{*} = 0.56$ For $D \leq 100$ mm, $W_G^{*1/2} + 0.88W_L^{*1/2} = 0.79$ $W_G^* = \left[\frac{\rho_G J_G}{Dg(\rho_L - \rho_G)} + \left(\frac{\mu_G J_G}{D^2 g(\rho_L - \rho_G)}\right)^{0.3}\right]^{1/2}$ $W_L^* = \left[\frac{\rho_L J_L^2}{Dg(\rho_L - \rho_G)} + \left(\frac{\mu_L J_L}{D^2 g(\rho_L - \rho_G)}\right)^{0.3}\right]^{1/2}$	The backflow water flow rate increases with the increase of pipe diameter for the same air flow rate
Dhar et al. [43] (2022)	Air–water	Rectangular channel width: 12; rectangular channel height: 50	1.72	0	$J_G^{*1/2} + J_L^{*1/2} = C$ $C \geq 0.86$	The effect of hydraulic jump on the transition from stratified flow to flooding and slugging in countercurrent and co-current flow was studied

Lots of experimental works were performed to investigate the flow patterns and flooding mechanisms on the horizontal countercurrent two-phase flow by visual observations. Ansari and Nariai [36] investigated the wave initiation and slugging occurrence of air–water countercurrent flow in a horizontal rectangular channel. They kept the test section horizontal and the water depth constant during the experiment, and different experimental tests were carried out by adjusting the water level in the tank. They observed three zones in the whole horizontal channel throughout different experimental tests (Figure 3). In the first zone, there is no wave growth, and the water surface is smooth, but the water surface appears to be vibrating. In the second zone, the waves with short wavelengths begin to grow. In the third zone, the slug takes place at a higher air flow rate. Two slug formation categories were proposed, namely slug initiation by short wavelength waves and slug initiation by mixed waves. A comparison of the two slugs showed that the slugs initiated by short wavelength waves create more severe situations and need a shorter transient period.

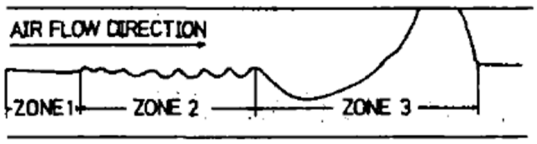

Figure 3. Conceptional view of the slug initiation (Ansari and Nariai [36]).

Wang and Kondo [37] carried out CCFL experiments in horizontal rectangular channels. They observed various air–water interface behaviors of CCFL for different liquid friction types. For $1 - \alpha < 0.25$, no slug forms in the horizontal channel. As the air velocity increases, a smooth flow transfers into a wave flow, then the water is stopped by the air flow, and CCFL occurs. For $0.25 < 1 - \alpha < 0.75$, CCFL occurs with a large wave growth and the slug flow onset. For $1 - \alpha > 0.75$, the smooth flow transfers to slug flow immediately.

In order to study the CCFL phenomenon in a nearly horizontal channel, Choi and No [38] conducted air–water CCFL experiments in nearly horizontal pipes. Two flooding mechanisms were proposed: inner flooding and entrance flooding (Figure 4). Inner flooding is initiated by sudden wave growth inside the pipe, and entrance flooding always happens at the water entrance without slugging. They also investigated the effects of pipe diameter, pipe end geometry, and inclination angle on CCFL. Results showed that the pipe diameter affects the inner flooding, but the influence of pipe diameter on the entrance flooding remains unclear. They found that the inclination angle has a great effect on CCFL, a slight increase of the inclination angle leads to a change of flooding onset location and the flow patterns. They also stated that the pipe end geometry has little effect on flooding within the tested range.

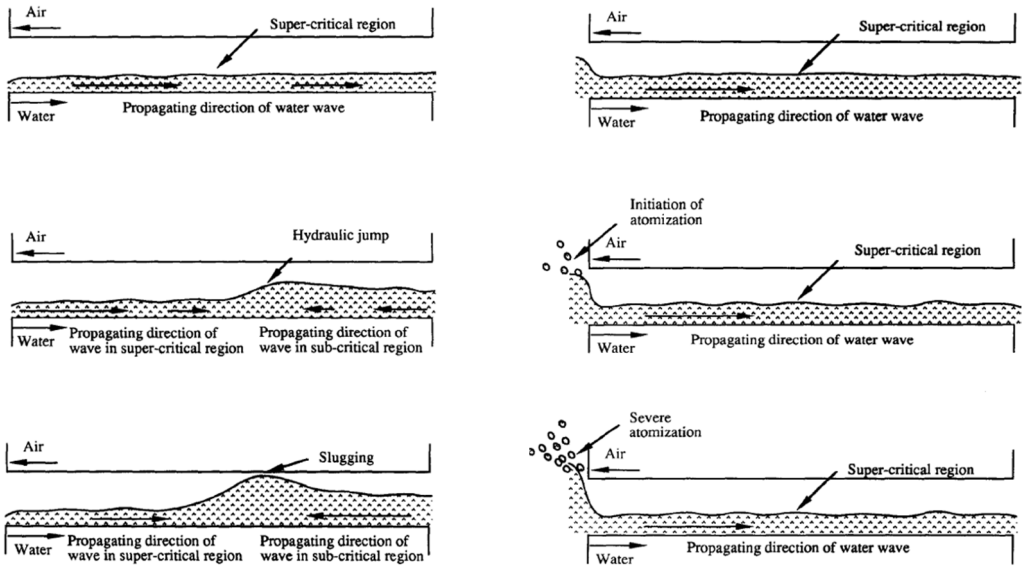

Figure 4. Flow patterns at different inclination angles: (**a**) $\theta = 0.69°$, (**b**) $\theta = 0.92°$ (Choi and No [38]).

A test facility named WENKA was designed to study the CCFL phenomenon and to identify the flow regimes in a simplified German PWR hot leg geometry. Gargallo et al. [41] performed air–water countercurrent flow experiments in the test facility. The horizontal test section in this test facility has a rectangular cross-section. They observed the two-phase flow phenomena of a hydraulic jump and flow reversal under different flow rates of air and water. They suggested that subcritical flow is necessary for the occurrence of flow reversal. The experimental results also validate the theoretical model, which is a 1D model presented to predict the CCFL. The flooding velocity was found to be sensitive to the inclination angle, which is also reported by Choi and No [38].

To evaluate the effect of pipe diameter on CCFL, Ma et al. [42] conducted countercurrent two-phase flow experiments with air and water in horizontal pipes. Results showed that the backflow water flow rate increases with the increase of pipe diameter for the same air flow rate. This is probably because the influence of the viscous force on the flow increases when the pipe diameter drops below a certain value. They proposed two CCFL correlations by using Wallis parameters and new dimensionless parameters W_K^*, which are applied to different pipe diameters.

For $D \geq 100$ mm,

$$J_G^{*1/2} + 0.388 J_L^{*1/2} + 0.49 J_L^* = 0.56 \tag{19}$$

For $D \leq 100$ mm,

$$\begin{aligned} W_G^{*1/2} + 0.88 W_L^{*1/2} &= 0.79 \\ W_G^* &= \left[\frac{\rho_G J_G}{D g(\rho_L - \rho_G)} + \left(\frac{\mu_G J_G}{D^2 g(\rho_L - \rho_G)} \right)^{0.3} \right]^{1/2} \\ W_L^* &= \left[\frac{\rho_L J_L^2}{D g(\rho_L - \rho_G)} + \left(\frac{\mu_L J_L}{D^2 g(\rho_L - \rho_G)} \right)^{0.3} \right]^{1/2} \end{aligned} \tag{20}$$

Dhar et al. [43] carried out gas–liquid flow experiments in a narrow rectangular channel to study the influence of hydraulic jump on the transition from stratified flow to flooding and slugging in countercurrent and co-current flow. They found that the occurrence of flooding is caused by the oscillatory jump. The hydraulic jump forms before the flooding takes place at the water inlet for supercritical liquid flow. The typical characteristics of a hydraulic jump in a narrow rectangular channel are shown in Figure 5.

The inception of the jump, also known as the "jump toe," is characterized by an abrupt rise in the air–water interface. The formation of the hydraulic jump is commonly associated with a "roller region" characterized by recirculation of the entrained air.

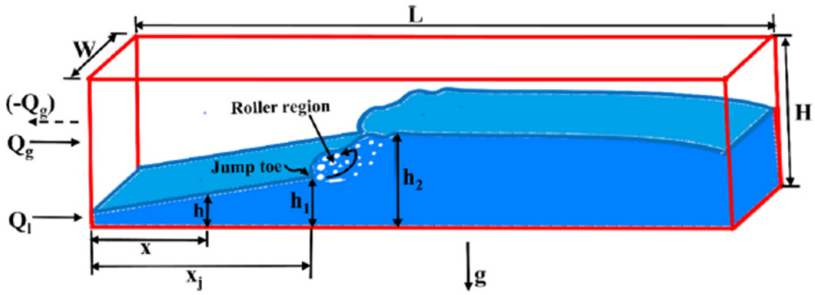

Figure 5. Schematic of internal hydraulic jump in a narrow rectangular channel (Dhar et al. [43]).

Note that the experimental investigations of two-phase countercurrent flow in horizontal channels mentioned above basically employed air and water as working fluids, there are also several studies dealing with steam and water [35,39,40]. Bankoff and Lee [35] carried out steam–water countercurrent flow experiments in a nearly horizontal rectangular channel to investigate the flooding mechanisms and the hysteresis effects. They found that the location of the occurrence of the onset of flooding depends on the water injection rate, and the onset of flooding can be classified into bottom flooding and top flooding. At low water flow rates, flooding initiated at the bottom of the test pipe, which is defined as bottom flooding. At high water flow rates, flooding took place at the top of the test pipe as a result of shearing off the crest of the liquid slug, which is defined as top flooding. They also observed the hysteresis effects owing to condensation during the partial delivery stage in the steam-water flow. Chun and Yu [39,40] performed a series of experiments to investigate the effect of steam condensation on CCFL in nearly horizontal pipes. Air–water and steam–water were used as working fluids. The results indicated that for a certain water flow rate, the gas flow rate required for the occurrence of CCFL for steam–water countercurrent flow is larger than that for air–water countercurrent flow.

3.3. Inclined Channel

As can be seen from the above review, a series of experimental investigations were carried out to study the CCFL in vertical and horizontal channels. The CCFL in inclined channels also potentially occurs under various situations in a PWR, such as the pressurizer surge line. Many studies were performed to investigate the CCFL phenomenon in the inclined channel and to explore the effect of inclination angle on CCFL, as shown in Table 3.

Lee and Bankoff [44] conducted steam–water countercurrent flow experiments in inclined rectangular channels. Different flooding characteristics were observed under different geometrical conditions by visual observations. For the channel depth $H = 38$ mm, the inclination angle $\theta = 4.5°$ and 33.5°, the onset of flooding is characterized by the formation of water slugs and bridging. The water slugs initiate at the water exit and then develop backward as the steam flow rate increases, leading to the rupture of the interface and the occurrence of bridging in the middle of the test channel. For $H = 76$ mm, $\theta = 4.5°$ and 2.9°, CCFL occurs with the appearance of roll waves and the formation of water slugs, but no backward propagation of a slug was observed. Instead, a mist of water droplets is entrained from the tops of the water slugs. Barnea et al. [45] observed two somewhat different flooding mechanisms of air–water countercurrent flow in an inclined circular pipe. They found that the onset of flooding occurs due to a local disturbance generated at the water entrance or the disturbance waves somewhere along the tube.

Table 3. Summary of the experimental investigations on the CCFL in inclined channels.

Authors	Test Fluids	Inner Pipe Diameter (mm)	Pipe Length (m)	Inclination Angle (°)	Remarks
Lee and Bankoff [44] (1983)	Steam–water	Rectangular channel width: 380; rectangular channel height: 38; 76	1.27	2.9, 4.5, 33.5	Different flooding characteristics were observed under different geometrical conditions by visual observations
Barnea et al. [45] (1986)	Air–water	51	10	1, 10, 20, 30, 40, 50, 70, 80, 90	Two different flooding mechanisms of air–water countercurrent flow were observed The effect of inclination angle on CCFL is not monotonic
Wongwises [46] (1998)	Air–water	29	3.5	60, 65, 70, 75, 80, 85	The effect of the inclination angle is of significance, but the effect is related to the upper end condition
Zapke and Kroger [47] (2000)	Air–water, air–propanol, air–methanol, argon–water, helium–water, helium–methanol, hydrogen–methanol	Rectangular channel width: 10, 20; rectangular channel height: 50, 100, 150	3.21	2, 5, 10, 15, 20, 40, 60, 70, 80, 90	The effects of liquid viscosity, surface tension, and phase densities on CCFL were examined The phase densities and channel sizes have a greater influence on CCFL than the liquid viscosity and surface tension The surface tension has less effect than the liquid viscosity
Deendarlianto et al. [48] (2010)	Air–water, air–0.02 wt.% oleic acid natrium solution, air–0.05 wt.% oleic acid natrium solution	16	1.1	30, 45, 60	The surface tension has a strong effect on flooding, especially at a high liquid flow rate
Prayitno et al. [49] (2012)	Air–water, air–30% glycerin aqua solution, air–50% glycerin aqua solution, air–2% butanol aqua solution, air–5% butanol aqua solution	50	1.1	10, 20	The flooding gas superficial velocities increase with increasing the inclination angle The liquid viscosity has a stronger influence on CCFL than the surface tension

In order to study the effect of inclination angle on the CCFL in an inclined channel, large numbers of flooding experiments were carried out [45,46,49]. Barnea et al. [45] performed air–water countercurrent flow experiments in inclined pipes with a whole range of inclination angles. They reported that the effect of inclination angle on CCFL is not monotonic. The flooding air flow rate increases and then decreases as the inclination angle changes from vertical to horizontal. They emphasized that a small deviation from the horizontal or the vertical position has a great influence on CCFL, which agree with the conclusions of Siddiqui et al. [50], Wan and Krishnan [51], and Choi and No [38]. Wongwises [46] stated that the effect of the inclination angle on CCFL is of significance, but the effect is related to the upper end condition. For an open upper end, the flooding air velocity increases with increasing the inclination angle. For a closed upper end, the flooding air velocity is independent of the inclination angle. Prayitno et al. [49] found the flooding gas velocity increases with the inclination angle increases. Note that the conclusion was obtained from only two different inclination angles.

The effects of fluid properties on CCFL are also of great interests in the investigations of countercurrent gas–liquid flow. Zapke and Kroger [47] used different combinations of test fluids to examine the effects of liquid viscosity, surface tension, and phase densities on CCFL. The results showed that the phase densities and channel sizes have a greater influence on CCFL than the liquid viscosity and surface tension, and surface tension has less effect than the liquid viscosity. In order to explore the effect of surface tension on flooding in an inclined pipe, Deendarlianto et al. [48] employed air and three different liquids as test fluids. They addressed that surface tension has a strong effect on flooding, especially at a high liquid flow rate. For high liquid flow rates, the upper flooding transfer into lower flooding with decreasing surface tension. Later, Prayitno et al. [49] studied the influence of the liquid properties on CCFL in an inclined pipe by using air and five different liquids as test fluids. The result indicated that the liquid viscosity has a stronger effect on CCFL than the surface tension, which was also proved by Zapke and Kroger [47].

In addition, many researchers observed that the gas/liquid entrance and exit conditions of the test section also significantly affect the CCFL in inclined channels [45,46]. Barnea et al. [45] found that the liquid entry method strongly affects the onset of flooding in an inclined pipe. Wongwises [46] noticed that the upper end condition has a strong effect on CCFL in a slightly inclined pipe.

3.4. Flow Channel with Elbow

The flow channels with elbow are wildly used in many scenarios in a PWR, such as the hot leg model and the pressurizer surge line model. The CCFL phenomena in these complex channels are more different from that in the simple geometries, namely vertical channels and horizontal channels. The experimental studies on CCFL in the flow channels with elbow are divided into three categories: typical hot leg model, pressurizer surge line, and other flow channel models with elbow.

3.4.1. Typical Hot Leg Model

The typical hot leg model in a PWR consists of a horizontal section, an inclined section, and an elbow connected the horizontal section to the inclined section as shown in Figure 6. Table 4 summarizes the experimental investigations on the CCFL in a PWR hot leg.

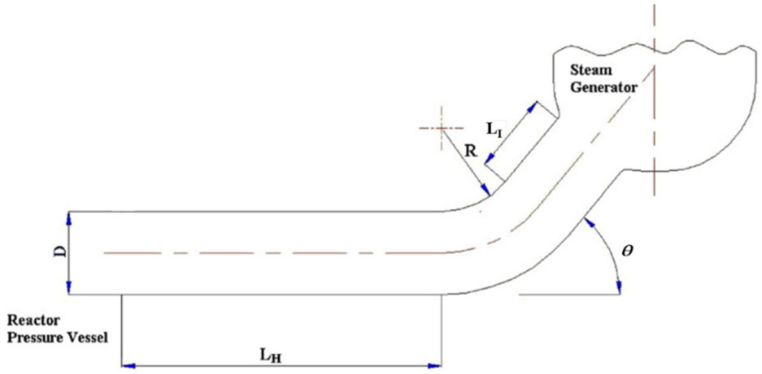

Figure 6. Typical hot leg geometry (Deendarlianto et al. [8]).

Table 4. Summary of the experimental investigations on the CCFL in the model of a PWR hot leg.

Authors	Test Fluids	Inner Pipe Diameter (mm)	Horizontal Leg Length (m)	Inclined Riser Length (m)	Inclination Angle (°)	Empirical Correlation	Remarks
Richter et al. [52] (1978)	Air–water	203	0.914	-	45	$J_G^{*1/2} + J_L^{*1/2} = 0.7$	The CCFL data was limited to the region of high air velocity Different CCFL mechanisms were observed
Ohnuki [53] (1986)	Air–water, steam–water	26–76	0.01–0.4	0.038–0.6	40, 45	$J_G^{*1/2} + 0.75J_L^{*1/2} = C$ For elliptical shapes of the upper air exit, $C = \ln\left\{\left(\frac{L_H}{D}\right)\left(\frac{1}{L_I}\right)\right\}^{-0.066} + 0.81$ For circular shapes of the upper air exit, $C = \ln\left\{\left(\frac{L_H}{D}\right)\left(\frac{1}{L_I}\right)\right\}^{-0.066} + 0.88$	The constant C is dependent on the horizontal pipe length, the inclined riser length, and the shape of the upper air exit, but C is independent of the shape of the elbow, the water head in the upper plenum, and the combination of fluids
Siddiqui et al. [50] (1986)	Air–water	36.5, 38, 44, 47	24D–95D	-	90	-	The inception of flooding with the slugging occurrence at the hydraulic jump forms in the lower leg close to the bend The tube diameter, the length and inclination of the horizontal leg, and the bend radius of curvature affect the flooding limit
Wan and Krishnan [51] (1986)	Air–water	51	58D	23D	89.75–90.35	-	The effect of the inclination of the lower leg is investigated A small inclination change of the lower leg strongly affects the flooding limit
Weiss and Hertlein [54] (1988)	Steam–water	750	9.47D	1.87D	50	-	The Wallis parameters seem to be able to perform the geometrical scaling of countercurrent flow in a PWR hot leg

Table 4. *Cont.*

Authors	Test Fluids	Inner Pipe Diameter (mm)	Horizontal Leg Length (m)	Inclined Riser Length (m)	Inclination Angle (°)	Empirical Correlation	Remarks
Mayinger et al. [55] (1993)	Steam–water	750	9.47D	1.87D	50	-	The falling water flow rate decreases with the increase of the steam flow rate The CCFL data at the two system pressure shows little discrepancy
Glaeser and Karwat [56] (1993)	Steam–water	750	9.47D	1.87D	50	$J_G^{*1/2} + mJ_L^{*1/2} = C_1 = C_2(\sin 40^\circ)^{1/4}$ $m = 0.7 \sim 1.0$, $C_1 = 0.61 \sim 0.75$	A Wallis-type correlation for different sizes of test facilities was proposed
Wongwises [54–56] (1994, 1996a, 1996b)	Air–water	64	8.7D–44D	1.3	50, 75, 90	-	The flooding mechanisms are dependent on the liquid flow rate The bend inclination angle, the water inlet conditions, and the horizontal pipe length show significant effects on the CCFL
Geffraye et al. [57] (1995)	Air–water	75, 351	2.473, 2.645	1.194, 1.060	50	-	The Wallis parameters could describe the CCFL point better than the Kutateladze parameters for a range of inner pipe diameters from 0.0254 to 0.75 m It is difficult to predict the CCFL in a PWR hot leg accurately
Kang et al. [11] (1999) Chun et al. [58] (1999)	Air–water	40, 80	0.7–3.388	0, 0.623, 0.648	0, 35	$J_G^{*1/2} + 0.397J_L^{*1/2} = 0.603 - 0.00234\frac{L_H}{D}$	The typical CCFL curve can be classified into three regions A lower air flow rate is required for CCFL with the longer horizontal pipe length, the larger horizontal pipe length-to-diameter ratio, and the higher initial water level
Navarro [2,59] (2005)	Air–water	36, 44, 54	0.1–0.8	0.1–0.5	30, 50, 70, 90	$J_G^{*1/2} + 0.2452J_L^{*1/2} + 1.17J_L^* = 0.5963$	The CCFL mechanisms depend on the liquid flow rate The effects of the horizontal pipe length, the inclined pipe length, the horizontal pipe length-to-diameter ratio, the bend inclination angle, and the water level in the upper tank were investigated
Deendarlianto et al. [1] (2008, 2011) Vallée et al. [60] (2009)	Air–water	Width × Gap for rectangular channel: 250 × 50	2.12	0.23	50	-	The onset of flooding initiates simultaneously with the formation of liquid slugs The system pressure affects the CCFL A hysteresis phenomenon was observed
Vallée et al. [61] (2011)	Air–water	Width × Gap for rectangular channel: 150 × 10, 250 × 50	1.24, 2.12	0.176, 0.23	50	-	The rectangular channel aspect ratio has an effect on the CCFL behavior The channel height is the characteristic length
Vallée et al. [62,63] (2012a, 2012b)	Air–water, Steam–water	Inner diameter for circular channel: 0.05 Width × Gap for rectangular channel: 250 × 50	0.43, 2.12	0.06, 0.23	50	-	A comparison between the air–water experiment and the steam–water experiment was made The Wallis parameters are correlated with the CCFL characteristics in a PWR hot leg over a wide range of system pressure An image-processing algorithm was developed
Montoya et al. [64] (2012)	Air–water, Steam–water	Width × Gap for rectangular channel: 250 × 50	2.12	0.23	50	-	An image-processing technique based on the experimental data images was developed
Lucas et al. [65] (2017)	Air–water, Steam–water	Width × Gap for rectangular channel: 250 × 50	2.2455	0.23	50	-	The discharged water flow rate and the ZP point slightly increase with the increase of system pressure The hysteresis phenomenon was observed
Minami et al. [66] (2010)	Air–water	50	0.43	0.06	50	$J_G^{*1/2} + 0.93\ J_L^{*1/2} = 0.68$	Two flow pattern maps by increasing and decreasing the air flow rate were obtained A hysteresis phenomenon exists in the flow pattern transition
Kinoshita et al. [67] (2011)	Air–water and Air–glycerol water solutions	50	0.43	0.06	50	-	The slope of the CCFL curve increases as the liquid viscosity increases, but the ZP point is independent of the liquid viscosity High-quality images of the air–water interfacial structure were acquired
Issa and Juan [68,69] (2013, 2014)	Air–water	190	1.8	0.355	50	-	Two main CCFL mechanisms, namely bend-CCFL and ADE-CCFL were observed The CCFL mechanisms are dependent on the inlet water velocities

Table 4. *Cont.*

Authors	Test Fluids	Inner Pipe Diameter (mm)	Horizontal Leg Length (m)	Inclined Riser Length (m)	Inclination Angle (°)	Empirical Correlation	Remarks
Issa and Juan [70] (2017)	Air–water	190	1.8	0.355	50	$J_G^{*1/2} + 0.47J_L^{*1/2} + 0.75J_L^* = 0.62$ $J_G^{*1/2} + 0.71J_L^{*1/2} = 0.63$ $J_G^{*1/2} = \begin{cases} 0.63 - 0.59J_L^{*1/2} & 0.02 < J_L^{*1/2} < 0.15 \\ 0.65 - 0.79J_L^{*1/2} & 0.15 < J_L^{*1/2} < 0.3 \end{cases}$	A new method of image processing time-averaged interface distributions was applied
Issa et al. [71] (2019)	Air–water	190, 50	1.8, 0.43	0.355, 0.06	50	-	The interface distributions at the water entrance/elbow/riser region cannot be scaled due to the effect of the pipe diameter on the CCFL mechanisms The criteria for obtaining CCFL data that can compare to the full-scale data was proposed
Badarudin et.al. [72,73] (2016, 2018)	Air–water	25.4	0.635, 1.27, 2.4	-	50		The flooding hysteresis phenomenon was observed Three different CCFL mechanisms were presented
Astyanto et.al [74] (2022)	Air–water	25.4	0.635	0.1	50	-	Some advanced statistical tools were used to clarify the flow characteristics

A series of experimental investigations were conducted in down-scale PWR hot leg models to explore the CCFL mechanisms and the various affecting factors of CCFL. Richter et al. [52] performed the air–water countercurrent experiments in a 3/10 scale model of a PWR hot leg, but their data was limited to the region of high air velocity. They correlated the obtained CCFL data by using the Wallis parameter. The Wallis-type correlation was proposed as below,

$$J_G^{*1/2} + J_L^{*1/2} = 0.7 \tag{21}$$

To investigate the CCFL characteristics of air–water and saturated steam–water flow, Ohnuki [53] conducted the experiments in a model of PWR hot leg. Note that most of the CCFL experiments were carried out by gradually increasing the air (or water) flow rate for a specified water (or air) flow rate, but the experiments in this study were carried out at quasi-steady conditions, in which the inclined pipe was covered with water and the water level in the upper water tank was constant. Ohnuki found that different CCFL mechanisms happened with various experimental tubes and different gas velocities. He stated that the constant C in Wallis-type correlation is dependent on the horizontal pipe length, the inclined riser length, and the shape of the upper air exit, but that the constant C is independent of the shape of the elbow, the water head in the upper plenum, and the combination of fluids. A Wallis-type correlation was proposed as follows,

$$J_G^{*1/2} + 0.75J_L^{*1/2} = C \tag{22}$$

where the constant C is a function of the horizontal pipe length-to-diameter ratio and the inclined riser length based on the experimental data, for elliptical shapes of the upper air exit,

$$C = \ln\left\{\left(\frac{L_H}{D}\right)\left(\frac{1}{L_I}\right)\right\}^{-0.066} + 0.81 \tag{23}$$

for circular shapes of the upper air exit,

$$C = \ln\left\{\left(\frac{L_H}{D}\right)\left(\frac{1}{L_I}\right)\right\}^{-0.066} + 0.88 \tag{24}$$

Siddiqui et al. [50] measured the flooding limits in the elbows between an upper vertical pipe and a lower horizontal or near horizontal pipe with air–water. They identified the inception of flooding with the slugging occurrence at the hydraulic jump forming in the lower leg close to the bend. They noticed that the gas flow rates at flooding were smaller when compared with vertical and horizontal pipes. The tube diameter, the length and inclination of the horizontal leg, and the bend radius of curvature were found to affect the flooding limit. They concluded that the air velocity of flooding decreases as the horizontal

leg length increases, greatly reduces with a slightly upward inclination of the horizontal pipe, and increases with a slight downward inclination of the horizontal pipe. However, the effects of bend radius of curvature and tube diameter on flooding are not fully understood.

Wan and Krishnan [51] conducted the air–water CCFL experiments in a 90° elbow with a slightly inclined lower leg. The experimental model is a simplified hot leg model of the CANDA pressurized heavy water reactor. The effect of the inclination of the lower leg was investigated. Results indicated that a small inclination change of the lower leg strongly affects the flooding limit, the less air flow rate is needed for the elbow with a lower upwardly inclined leg compared with a horizontal leg, while the elbow with a lower downwardly inclined leg requires a larger air flow rate. The results were in good agreement with the conclusions of Siddiqui et al. [50].

Wongwises [75–77] investigated the two-phase CCFL in a bend between a horizontal pipe and an inclined pipe experimentally. Air and water were employed as working fluids in this experiment. Different flooding mechanisms were observed from the visual observation. They found that the flooding mechanisms are dependent on the water flow rate, and the typical flooding curve can be divided into three regions as shown in Figure 7.

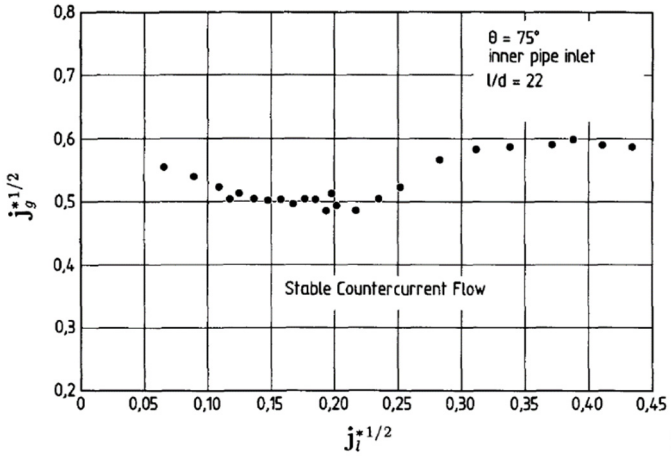

Figure 7. Typical flooding curve (Wongwises [75]).

In the first region ($J_L^{*1/2} < 0.2$), CCFL decreases with the increase of the liquid flow rate. The thin hydraulic jump appears to be close to the elbow at low liquid flow rates, and the hydraulic jump gets bigger and moves away from the elbow as the liquid flow rate increases. In this region, CCFL occurs simultaneously with the slugging of the unstable waves forming at the crest of the hydraulic jump. In the second region ($0.2 < J_L^{*1/2} < 0.5$), CCFL increases as the liquid flow rate increases, and the hydraulic jump appears near the water outlet. They observed two different phenomena in this region. For $J_L^{*1/2}$ values slightly greatly than 0.2, the injected water is pushed ahead like a froth slug by the air with high velocity, and the bridging occurs inside the horizontal pipe near the elbow. For $J_L^{*1/2} > 0.2$, the air pushes the slug upstream swiftly, and the bridging appears far away from the lower pipe of the elbow. In the third region ($J_L^{*1/2} > 0.5$), CCFL decreases with the increase of the liquid flow rate. In this region, CCFL happens as a result of the slug formation at the end of the horizontal leg, and no hydraulic jump is observed. They also reported that the bend inclination angle, the water inlet conditions, and the horizontal pipe length show significant effects on the CCFL.

Geffraye et al. [57] presented a study on the prediction of CCFL and analyzed the experimental data under the MHRESA experimental program. Two different test sections of the hot leg model were employed, and air and water were used as the working fluids. They focused on the ZP point in the experiments, and noticed the ZP point is 0.52 when the inner pipe diameter is 0.075 m and 0.61 when the inner pipe diameter is 0.351 m. They found that the Wallis parameters could describe the CCFL point better than the Kutateladze

parameters for a range of inner pipe diameters from 0.0254 to 0.75 m. They also proposed that it is difficult to predict the CCFL in a PWR hot leg accurately because many various parameters may affect the onset of flooding.

Kang et al. [11] and Chun et al. [58] carried out air–water CCFL experiments to investigate the CCFL characteristics and the effects of various experimental factors on the CCFL. The test section in the experiment simulated a PWR hot leg of the Korean standard nuclear power plant. They proposed that the CCFL phenomenon can be divided into three categories: the onset of flooding, the partial liquid delivery, and the zero liquid penetration (Figure 2). The onset of flooding is dependent on the inlet water flow rate, and the ZP point is independent of the water flow rate.

The typical CCFL curve obtained with a hot leg model by using Wallis parameters can be classified into three regions as Figure 8 shows. For $J_L^{*1/2} < 0.2$, the transition from supercritical flow to subcritical flow occurs in the horizontal pipe, and a hydraulic jump appears. The water flow rate influences the location of the hydraulic jump, the location shifts away from the elbow at higher water flow rates and shifts closer to the elbow at lower water flow rates. For $0.2 < J_L^{*1/2} < 0.4$, the flow comprises supercritical flow, and no hydraulic jump occurs in the horizontal pipe. Large numbers of small water droplets are entrained in the upper region of the pipe, and large amplitude roll-waves develop near the end of the horizontal pipe when the CCFL occurs. For $0.4 < J_L^{*1/2} < 0.7$, no hydraulic jump occurs in the horizontal pipe and no water layer depth increases at the end of the horizontal pipe. The active entrainment of water droplets into the water vessel leads to the CCFL, which occurs at the inlet of the inclined pipe.

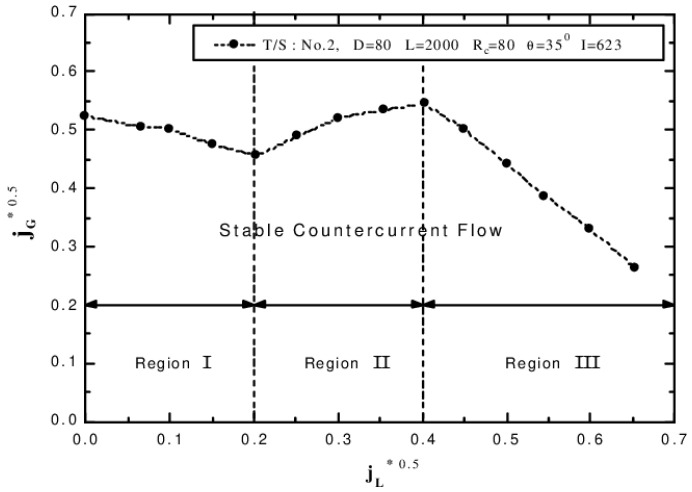

Figure 8. Typical CCFL curve (Kang et al. [11]).

Kang et al. also explored the effects of geometrical parameters and the initial water level in the horizontal pipe on CCFL. They found that a lower air flow rate is required for CCFL with the longer horizontal pipe length, the larger horizontal pipe length-to-diameter ratio, and the higher initial water level. They proposed a Wallis-type correlation based on the experimental data in the low inlet water flow rate region, which agrees more closely with the existing CCFL data of large diameter pipes than the correlation of Ohnuki [53]. The Wallis-type correlation was correlated as below.

$$J_G^{*1/2} + 0.397 J_L^{*1/2} = 0.603 - 0.00234 \frac{L_H}{D} \quad (25)$$

Later, Kim and No [78] obtained a new CCFL empirical correlation based on a total of 356 experimental datapoints from previous experimental works. The Wallis-type correlation shows the effect of the length-to-diameter ratio and is expressed by:

$$(J_G^*)^{1/2} + 0.614(J_L^*)^{1/2} = 0.635 - 0.00254\left(\frac{L_H}{D}\right) \tag{26}$$

Navarro [2,59] conducted experiments with air and water in a PWR hot leg model to study the CCFL phenomenon. Navarro found that the CCFL mechanisms depend on the water flow rate. For low water flow rates, the formation of a hydraulic jump leads to CCFL, and the CCFL occurs in the horizontal pipe close to the elbow. For an intermediate water flow rate, CCFL occurs at the lower end of the horizontal pipe with the formation of a slug. For high water flow rates, the area reduction to the air flow leads to CCFL, and the CCFL occurs at the upper extremity. Navarro investigated the effects of various geometric parameters on CCFL by the partial CCFL data. Results showed that when the horizontal pipe length increases, the critical air velocities and zero liquid penetration decrease. The critical air velocity rarely decreases as the inclined pipe length increases, and the inclined pipe length almost does not affect the ZP point. The CCFL curves created by using Wallis parameters show little differences for different horizontal pipe length-to-diameter ratios, due to these two ratios being similar. A slight reduction in the air velocity to the ZP point ratio was observed as the bend inclination angle increased. There were few differences among the CCFL curves when the bend inclination angles were 30°, 50° and 70°, and the critical air velocity decreases when the bend inclination angle increases to 90°. As the pipe diameter decreases, the critical air velocity decreases. This conclusion may be questionable because only two different pipe diameters were employed. When the water head of the upper tank is lower than 4 cm, there is no difference between the CCFL curves, and the critical air velocity decreases for the water level larger than 4 cm. Navarro correlated a quadratic correlation in terms of the Wallis parameters based on the partial CCFL data, which is a function of the horizontal pipe length, the inclined pipe length, the pipe diameter, the bend inclination angle, and the water level of the upper tank. When the correlation is applied to a PWR hot leg model, it can be written in a simpler form as follows:

$$J_G^{*1/2} + 0.2452J_L^{*1/2} + 1.17J_L^* = 0.5963 \tag{27}$$

Minami et al. [66] studied the CCFL characteristics and the flow patterns of the whole process before and after the onset of flooding in a model of 1/15 scale of the actual PWR hot leg. Higher-resolution images of air-water countercurrent flow patterns are obtained. The experimental setup and experimental procedure are similar to that of Navarro [2]. They obtained two flow pattern maps by increasing and decreasing the air flow rate, and the flow pattern maps contain different flow patterns as Figure 9 shows. The correspondence of flow patterns to the numbers is shown in Table 5. It can be seen that these two flow pattern maps have large differences. A hysteresis phenomenon exists in the flow pattern transition, the air velocity which is needed for the transition from wavy flow to stratified flow, where the decreasing air velocity is lower than is necessary for the transition from stratified flow to wavy flow. Minami et al. stated that the CCFL characteristics are closely related with the flow patterns. Flow patterns in the horizontal pipe near the bend have a great effect on those in the bend and the inclined pipe. They found that the CCFL characteristics obtained by decreasing the air flow rate follow a linear relationship and are independent of the inlet water flow rate, which was also reported by Navarro [2,59]. The Wallis-type correlation obtained by decreasing the air flow rate was proposed as follows:

$$J_G^{*1/2} + 0.93J_L^{*1/2} = 0.68 \tag{28}$$

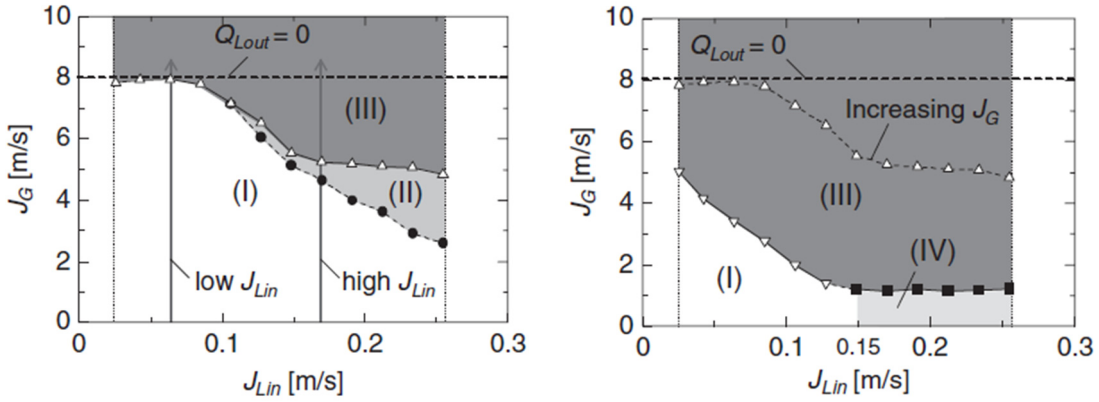

(**a**) (**b**)

Figure 9. Flow pattern map: (**a**) for increasing the gas flow rate, (**b**) for decreasing the gas flow rate (Minami et al. [66]).

Table 5. Correspondence of flow patterns to the numbers shown in Figure 9 (Minami et al. [66]).

Number	Horizontal Section	Elbow	Inclined Section
(I)	Stratified	Stratified	Stratified
(II)	Positive wavy flow	Positive wavy flow	Positive wavy flow
(III)	Negative wavy flow	Annular-mist	Annular-mist
(IV)	Oscillatory	Oscillatory	Oscillatory

To study the effects of liquid properties on CCFL, Kinoshita et al. [67] conducted two-phase countercurrent flow experiments in the same experimental facility as Minami et al. [66]. The test fluids were air–water and air–glycerol water solutions. They stated that the slope of the CCFL curves correlated by Wallis parameters increases as the liquid viscosity increases, but the ZP point is independent of the liquid viscosity. The reason was that the liquid viscosity has an influence on the wall friction force but does not influence the interfacial drag.

Issa and Juan carried out a series of investigations upon CCFL with air–water in a 1/3.9 scale of hot leg model of the COLLIDER test facility [68–71]. They studied the mechanisms and flow patterns of the onset of flooding and deflooding [68,69]. High-quality images of the air–water interfacial structure were acquired by high-speed recordings, which are valuable for CFD validation, and the CCFL data enriched the CCFL data bank for large-diameter pipes. Note that the flow rate of the falling water into the reactor vessel simulator was no longer measured through the rate of water rise in the reactor vessel simulator. The falling water flow rate was measured by a flow meter in this experiment, which is more accurate than previous experiments. They observed two main CCFL mechanisms: bend-CCFL and ADE-CCFL, and the mechanisms are dependent on the inlet water velocities. Four regions were divided according to the inlet water velocity. For the first region ($0.085 < J_L^{*1/2} < 0.125$), the bend-CCFL appears near the elbow gradually (Figure 10). For the second region ($0.135 < J_L^{*1/2} < 0.175$), a sudden bend-CCFL occurs in this region. For the third region ($0.185 < J_L^{*1/2} < 0.265$), a dual-mode CCFL appears with the occurrence of slight ADE-CCFL and sudden bend-CCFL. For the fourth region ($0.275 < J_L^{*1/2} < 0.305$), there exists a dual-mode CCFL with the occurrence of strong ADE-CCFL and sudden occurrence of intense bend-CCFL (Figure 11).

Figure 10. The onset of bend-CCFL in the first region. $J_L^{1/2} = 0.105$ (Issa and Juan [69]).

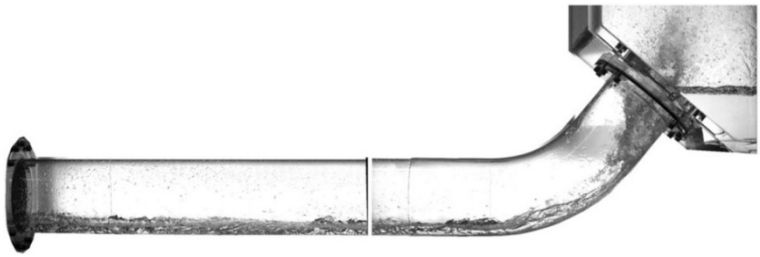

Figure 11. The air/water interface during the onset of ADE-CCFL in the fourth region. $J_L^{*1/2} = 0.305$ (Issa and Juan [69]).

To investigate the CCFL characteristics deeply, Issa and Juan [70] applied a new method of image-processing of time-averaged interface distributions. This new method is able to show the average repetitive behavior of the chaotic interface and emphasize important details, making it possible to compare with other experiments. They suggested that the CCFL phenomena cannot be predicted accurately using 1D models because the 1D models are unable to consider the spatial distribution of the gas–liquid interface. They obtained the CCFL characteristics by decreasing the air velocity. The CCFL correlations in terms of Wallis parameters were proposed by a quadratic relationship and a linear relationship, respectively, as below.

$$J_G^{*1/2} + 0.47J_L^{*1/2} + 0.75J_L^{*} = 0.62 \quad 0.02 < J_L^{*1/2} < 0.3 \tag{29}$$

$$J_G^{*1/2} + 0.71J_L^{*1/2} = 0.63 \quad 0.02 < J_L^{*1/2} < 0.3 \tag{30}$$

To fit the full range using liner correlations, a piecewise liner CCFL correlation was presented as:

$$J_G^{*1/2} + 0.59J_L^{*1/2} = 0.63 \quad 0.02 < J_L^{*1/2} < 0.15 \tag{31}$$

$$J_G^{*1/2} + 0.79J_L^{*1/2} = 0.65 \quad 0.15 < J_L^{*1/2} < 0.3 \tag{32}$$

Later, Issa and Juan [71] compared the CCFL data with those in the COLLIDER 1/4 and Kobe 1/15 scaled hot leg models. Results showed that the interface distributions at the water entrance/elbow/riser region cannot be scaled due to the effect of the pipe diameter on the mechanisms of CCFL occurrence. They proposed the criteria for obtaining CCFL data that can compare to the full-scale data: (a) $\frac{L_H}{D} \approx 9.47$, $\frac{L_I}{D} \approx 1.87$, $\theta = 50°$. (b) The liquid inlet should be rounded and smooth to avoid additional disturbance of the liquid flow. (c) The hydraulic diameter must be sufficiently larger than 50 mm to extrapolate the CCFL characteristics of the full-scale hot leg.

Badarudin et al. [72,73] investigated the air–water flooding and deflooding phenomena in a 1/30 scale of hot leg of the German Konvoi type reactor. The flooding hysteresis phenomenon was observed, which was also reported by Deendarlianto et al. [1], Minami et al. [66], and Issa and Juan [69], and the flooding hysteresis phenomenon is more significant at higher water velocities. They determined the liquid film thickness in the horizontal pipe by using processed images to study the interfacial behavior of flooding and deflooding. Three different CCFL mechanisms were presented. At low water velocity, the wavy

air–water interface along the horizontal pipe in the form of a liquid blockage on the bend leads to the onset of flooding. At medium water velocity, the slug occurs at the horizontal pipe, but the slug immediately collapses due to insufficient water to maintain the blockage. At high water velocity, the slug occurs and moves along the horizontal pipe until the bend. They grouped the CCFL data into three regions in terms of the water superficial velocity, which is similar to that of Wongwises [75] and Kang et al. [11]. For $J_L^{*1/2} \leq 0.24$, CCFL decreases as the water velocity increases. For $0.24 \leq J_L^{*1/2} \leq 0.34$, CCFL is independent of the water velocity. For $J_L^{*1/2} > 0.34$, CCFL decreases with the increase of the water velocity. They found that the location of the slug occurrence is dependent on the water velocity, and that the distance between the slugging position and the water outlet increases with the increase of the water velocity. They also studied the effect of the horizontal pipe length on the onset of flooding.

Astyanto et al. [74] conducted air–water countercurrent flow experiments in a 1/30 down-scaled hot leg of the Germany Konvoi type reactor and studied the statistical characteristics of the liquid film thickness fluctuations measured by resistive-conductance probe signals. To clarify the flow characteristics, some advanced statistical tools were used, such as PDF, PSDF, Kolmogorov entropy, and wavelet transform. Results indicated that the flow development during flooding is related to the liquid film thickening combined with the interface instability, which is caused by the increase of the air discharge. This causes a liquid blockage, which initiates the CCFL, and then the slug and churn flow occur. They proposed that the low dominant frequency corresponds to the onset of either liquid blockage or slugs, whereas the largest scale fluctuations reveal the wave movements.

It is noteworthy that the experimental investigations on CCFL in the PWR hot legs mentioned above were all carried out in circular cross-section channels. Compared with rectangular channels, the distribution obtained by a side-view projection in circular channels is more complex due to the additional distribution over the cross-sectional area. Therefore, in order to avoid the limitation of the 3D shape of the interfacial structure, Deendarlianto and his co-workers carried out their experimental investigations in a rectangular channel of a PWR hot leg model. The height and the width of the rectangular channel were 0.25 m and 0.05 m, respectively. The hot leg model representing the German Konvoi PWR hot leg at a scale of 1:3 was installed at the TOPFLOW facility [1,61–66].

Deendarlianto et al. [1] and Vallée et al. [60] studied the flow behavior before and after the onset of flooding at low and high water flow rates. During a flooding experiment, three regions were divided into: the stable countercurrent flow region, the partial delivery region, and the zero liquid penetration region, as shown in Figure 12. They found that the onset of flooding initiates simultaneously with the formation of liquid slugs, which develop near the elbow. The system pressure affects the CCFL, and the air flow rate needed to initiate CCFL increases with the increase of the system pressure. A hysteresis phenomenon was found between the flooding and deflooding experiments, and the hysteresis effect is stronger at a higher water flow rate. According to comparing the experimental data with those in previous literature, they found that the Wallis parameters can be applied to rectangular cross-sections by using the channel height as the characteristic length.

Vallée et al. [61] compared the CCFL experiments in the hot leg model at the TOPFLOW facility with that at Kobe University. The hot leg model at Kobe University has a rectangular cross-section with a width of 0.01 m and a height of 0.15 m. The comparison indicated that the CCFL behaviors in the two hot leg models are similar. The CCFL data of TOPFLOW facility fit better with previous CCFL data than that of Kobe facility, CCFL occurs at lower air flow rates in the narrow channel of Kobe facility. The result indicated that the channel aspect ratio has an effect on the CCFL behavior, which was already reported in small scale hot legs with circular cross-sections. Besides, the same conclusion as Deendarlianto et al. [1] was obtained, in which the channel height is the characteristic length used in the Wallis parameters for rectangular channels. Later, Vallée et al. [62] conducted the two-phase countercurrent flow experiments with air–water and steam–water in the hot leg model. Results showed that there might remain a small difference between the air–water

experiment and the steam–water experiment. They also developed an image-processing algorithm in order to capture the detailed gas–liquid interface in the camera images. Vallée et al. [63] also made a comparison between the air–water experiment and the steam–water experiment in detail. The result indicated that the steam is probably wet due to heat losses and liquid entrainment from the heater circuit. They confirmed that the Wallis parameters are correlated with the CCFL characteristics in a PWR hot leg over a wide range of system pressures and temperature conditions.

Montoya et al. [64] developed an image-processing technique to study the interfacial behavior of the air–water and steam–water countercurrent flow based on the experimental data images. Quantitative local flow information can be acquired using this technique. Statistical tools were also used to identify the flow behaviors. They suggested that the data obtained by using these advanced methods can be used to verify the CFD code.

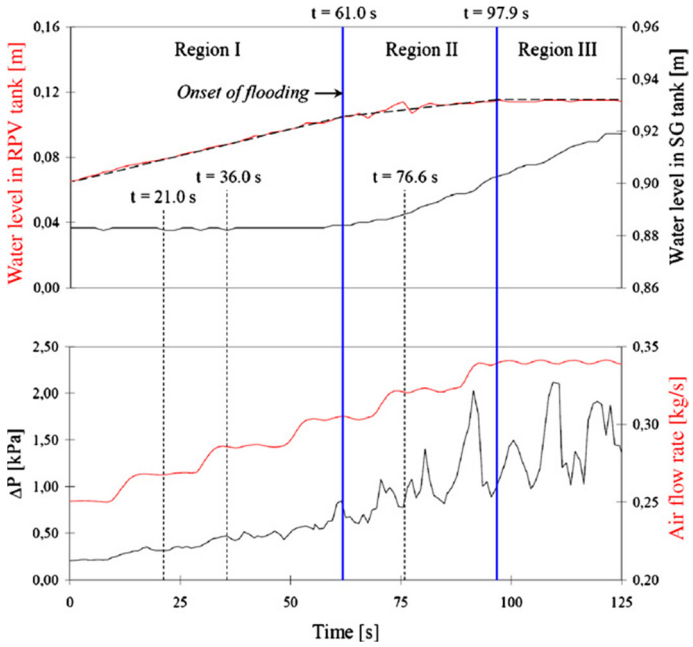

Figure 12. Variation of water level in the SG separator and in the RPV simulator, and of the pressure difference between the vessels and of the air mass flow rate measured at a water mass flow rate $\dot{m}_L = 0.3$ kg/s (Deendarlianto et al. [1]).

Lucas et al. [65] investigated the steady state CCFL characteristics in the hot leg model. They found that the discharged water flow rate and the ZP point slightly increase with the increase of system pressure, which is consistent with Deendarlianto et al. [1]. The hysteresis phenomenon was also observed in the experiments. They analyzed the slug frequencies according to the pressure measurements along the horizontal pipe, and the results indicated that the slug frequencies increase with the system pressure and decrease with the air flow rate.

D'Auria and Galassi [79] proposed that the CCFL phenomena strongly depend upon the geometrical scales. It is uncertain whether the downscaled hot leg models can represent the actual models properly. Glaeser and Rohatgi [80] presented some experimental results to illustrate the scaling dependence of countercurrent flow in the hot leg, the downcomer, and the upper core tie plate. They found that the flow phenomena in full-size models are very different from that in downscaled facilities, and the CCFL correlations developed from downscaled facilities are not applicable any more. Thus, the CCFL data based on the full-scale hot leg model are needed to investigate the CCFL phenomena in a PWR hot leg model. In order to investigate the CCFL phenomena and provide CCFL data in full-scale PWR hot leg, some experiments were carried out at the upper plenum test facility (UPTF) [54–56].

Weiss and Hertlein [54] found that the Wallis-type correlations of Richter et al. [52] and Ohnuki [53] agree very well with the data of UPTF test facility, and the Wallis parameters seem to be able to perform the geometrical scaling of countercurrent flow in a PWR hot leg. Mayinger et al. [55] performed the countercurrent flow experiment at the UPTF facility under two system pressures, 3 bar and 15 bar. They found that the falling water flow rate decreases with the increase of the steam flow rate. The CCFL data at the two system pressure show little discrepancy, which indicates that the Wallis parameters adequately account for pressure effects (Figure 13).

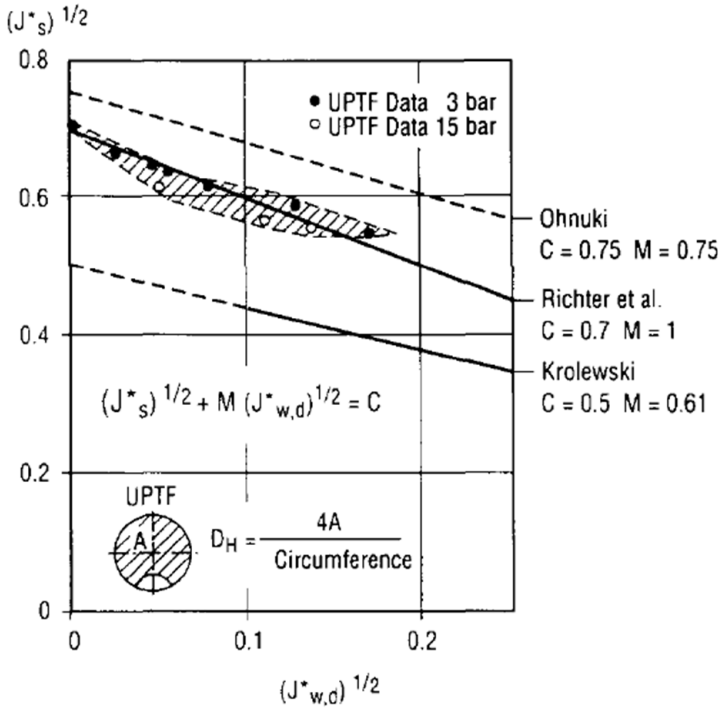

Figure 13. UPTF test data (Mayinger et al. [55]).

Glaeser and Karwat [56] proposed that the Wallis-type correlation for different sizes of test facilities can be correlated as below,

$$J_G^{*1/2} + mJ_L^{*1/2} = C_1 = C_2(\sin 40^\circ)^{1/4} \tag{33}$$

with $m = 0.7 - 1.0$ and $C_1 = 0.61 - 0.75$.

3.4.2. Pressurizer Surge Line Model

During a SBLOCA, the CCFL phenomenon probably takes place in the pressurizer surge line of a PWR, which will restrict the draining of water from the pressurizer. It is important to predict the pressurizer draining because the gravity head in the pressurizer affects the pressure in the downcomer. The pressurizer surge line consists of a vertical pipe, a vertical elbow, and an inclined pipe with several elbows as Figure 14 shows. It is difficult to predict the CCFL in the surge line accurately due to its complex geometry. Therefore, the CCFL data and knowledge obtained from simple geometries are not applicable anymore. Many researchers carried out experimental investigations in the model of a PWR pressurizer surge line in recent years as shown in Table 6.

Takeuchi et al. [81] compared the CCFL at different sections to determine which section is most limiting. They stated that the CCFL in the vertical section is the most dominant. Futatsugi et al. [82] carried out countercurrent flow experiments with air and water in a 1/10 downscaled model of a PWR pressurizer surge line. The inner diameter of the surge line was 30 mm. The results showed that CCFL occurs at three different locations,

i.e., at the upper junction (CCFL-U), in the surge line (CCFL-S), and at the lower junction (CCFL-L), the CCFL characteristics are governed by the most limiting one. The effects of inclination angle and the presence of elbows were also studied. They found that the effect of inclination angle on CCFL depends on the flow direction, and the presence of elbows leads to the increase of the flow limitation, while the flow limitations at the upper junction and the lower junction are independent of the presence of elbows.

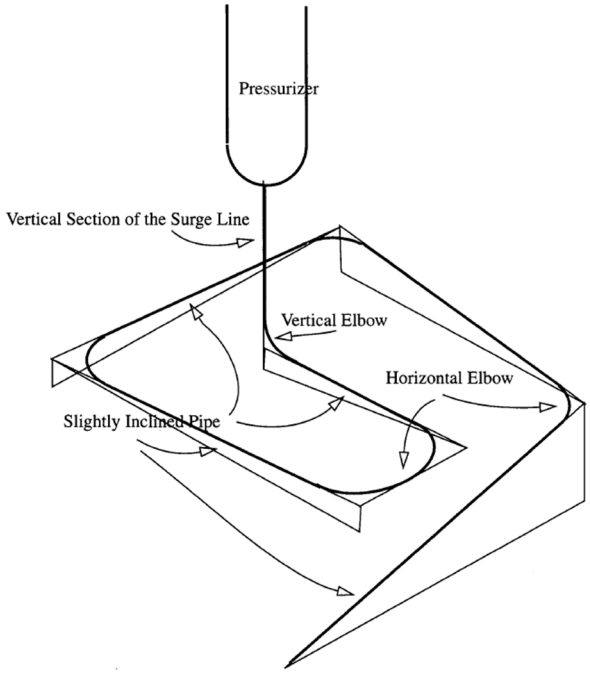

Figure 14. A model of a pressurizer surge line (Takeuchi et al. [81]).

Table 6. Summary of the experimental investigations on the CCFL in the PWR pressurizer surge line.

Authors	Test Fluids	Inner Pipe Diameter (mm)	Empirical Correlation	Remarks
Takeuchi et al. [81] (1999)	-	-	-	The CCFL in the vertical section is the most dominant
Futatsugi et al. [82] (2012)	Air–water	30	-	CCFL occurs at three different locations, and the CCFL characteristics are governed by the most limiting one The effects of the inclination angle and the presence of elbows were studied
Yu et al. [4,83] (2016, 2018a)	Air–water	90	For $0 < h_{HL} < 0.5D$, $Ku_L^{*1/2} + 1.075Ku_G^{*1/2} = 1.451$ For $h_{HL} = 0.75D$ $Ku_L^{*1/2} + 2.53Ku_G^{*1/2} - 1.64Ku_G^{*} = 0.99$	The CCFL mainly occurs in three different sections The development process of the CCFL was divided into four regions Two entrainment flow regimes were observed
Yu et al. [84] (2018b)	Steam–water	90	$Ku_G^{*1/2} + 1.05Ku_L^{*1/2} = 1.16 \pm 0.06$	The development process of the CCFL was divided into four regions The water level in the pressurizer simulator slightly affects the countercurrent flow process
Takaki et al. [85] (2020)	Air–water, steam–water	30–90	$Ku_G^{*1/2} + 0.79Ku_L^{*1/2} = 1.20 \pm 0.20$	The effects of fluid properties were evaluated

Yu et al. conducted a series of experimental investigations in a 1/4 downscaled PWR pressurizer surge line model to study the CCFL characteristics and the entrainment effect in the surge line [4,83,84]. In their experiments, the inner pipe diameter was 90 mm. They first conducted air–water countercurrent experiments in the whole-visual test section at ambient pressure and temperature [4]. They observed that the CCFL mainly occurs in three different sections, that is, in the section from the upper junction to the vertical elbow (CCFL-U), at the lower junction (CCFL-L), and in the inclined section of the surge line

(CCFL-S). The CCFL in the pressurizer surge line is determined by the most dominant CCFL-U, which was also reported by Takeuchi et al. [81], and Yamamoto et al. [86]. They divided the development process of the CCFL into four regions as shown in Figure 15.

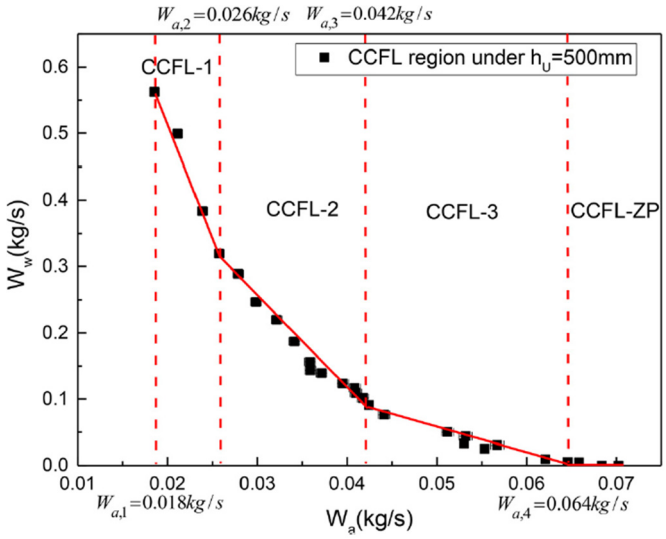

Figure 15. Definition of flooding region (Yu et al. [4]).

In the CCFL-1 region, only CCFL-U occurs; in the CCFL-2 region, CCFL-U and CCFL-S take place simultaneously; there are the occurrences of CCFL-U, CCFL-S, and CCFL-L in the CCFL-3 region; CCFL-U and CCFL-H take place in the CCFL-ZP region. The effect of the water level in the pressurizer simulator on CCFL was also studied. The results show that the effect on CCFL is strong when the water level is high and the air flow rate is low, and that the effect is small when the air flow rate is high and near the condition of ZP. They also demonstrated that the CCFL characteristics for simple geometries and the surge line model with small diameters cannot be applied to the CCFL prediction in the pressurizer surge line. On the basis of this experimental work, Yu et al. [83] continued to perform air–water countercurrent experiments to investigate the entrainment effect on CCFL in the hot leg and surge line assembly. They observed two entrainment flow regimes: stratified-flow entrainment and slug-flow entrainment, and the two flow regimes were found to take place in the hot leg and surge line assembly under certain hot leg water levels and air flow rate conditions. They proposed two empirical correlations of partial CCFL for different hot leg water levels h_{HL} by using Kutateladze numbers.

For $0 < h_{HL} < 0.5D$,

$$Ku_L^{*1/2} + 1.075Ku_G^{*1/2} = 1.451 \qquad Ku_G^* > 0, Ku_L^* > 0 \tag{34}$$

For $h_{HL} = 0.75D$,

$$Ku_L^{*1/2} + 2.53Ku_G^{*1/2} - 1.64Ku_G^* = 0.99 \qquad 0.09 < Ku_G^* < 0.64 \tag{35}$$

Later, Yu et al. [84] steam–water countercurrent experiments in a stainless-steel test section under normal pressure and saturated temperature conditions. The development process of CCFL can also be divided into four regions as Figure 16 shows. Compared with the CCFL development process in the air–water experiment, the process in the steam–water experiment is basically the same except for the CCFL-ZP region, in which only CCFL-U takes place. The water level in the pressurizer simulator slightly affects the countercurrent flow process, which is different from that in the air–water experiment [4]. They noticed that the CCFL characteristic is dependent on the experimental methods, test fluids, test

section assembly, and condensation effect. A partial CCFL empirical correlation in terms of Kutateladze numbers based on experimental data was proposed below.

$$Ku_G^{*1/2} + 1.05Ku_L^{*1/2} = 1.16 \pm 0.06 \qquad 0.7 \leqslant Ku_G^{*1/2} \leqslant 1.15, Ku_L^{*1/2} \geqslant 0 \tag{36}$$

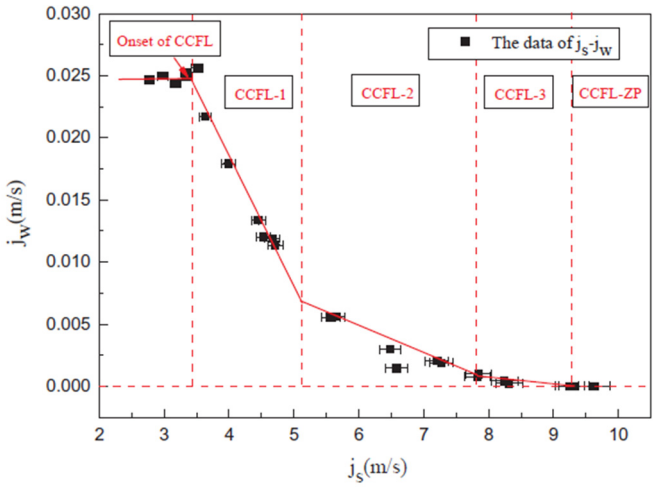

Figure 16. The development process of CCFL (Yu et al. [84]).

Takaki et al. [85] evaluated the effects of fluid properties on CCFL by using the data of vertical pipes. The results indicated that the density ratio is better than the viscosity ratio for evaluating CCFL-U as an affecting factor. They analyzed the surge line CCFL data of previous experimental works (Takeuchi et al. [81], Futatsugi et al. [82], Yu et al. [4,84]) and obtained a CCFL correlation of the surge line by using Kutateladze numbers as follows.

$$Ku_G^{*1/2} + 0.79Ku_L^{*1/2} = 1.20 \pm 0.20 \tag{37}$$

3.4.3. Other Flow Channel Models with an Elbow

As can be seen, numerous experimental works have been carried out to investigate the CCFL phenomena in simple geometries (e.g., vertical channels and horizontal channels), the PWR hot leg, and the pressurizer surge line. In order to study the CCFL mechanisms and characteristics in some more complex geometries, such as in a flow channel with multiple elbows or an inclined channel with rising elbow, some researchers conducted two-phase CCFL experimental works, which are summarized in Table 7.

Table 7. Summary of the experimental investigations on the CCFL in other flow channels with elbows.

Authors	Test Fluids	Test Models	Inner Pipe Diameter (mm)	Remarks
Krolewski [87] (1980)	Air–water	Flow channel with two elbows	51	The geometry of the test section affects the CCFL significantly The hysteresis range is very high for two of the test configurations
Kawaji et al. [88,89] (1989, 1991)	Air–water	Vertical-to-downwardly inclined pipes	51	Different CCFL mechanisms at various water flow rates were observed The formation of a hydraulic jump in the horizontal pipe near the bend has a significant effect on flooding
Ghiaasiaan et al. [90] (1994)	Air–water	Inclined flow channel connected to elbows in both ends	19	The experiments were performed with constant water-head liquid injection No hysteresis phenomenon was observed
Ghiaasiaan et al. [91] (1997)	Air–water, air–mineral oil, air–paraffinic oil	Inclined flow channel connected to elbows in both ends	19	The influences of liquid properties were evaluated

Krolewski [87] performed flooding experiments for air–water countercurrent flow in a complex test model with two elbows. The test model was composed of two elbows and a horizontal pipe, which was connected to vertical/inclined pipes in the two ends. The inner diameter of the test flow channel was 51 mm. Five different experimental configurations were tested in the experiments. The result showed that the geometry of the test section affects the CCFL significantly. The hysteresis range is very high for two of the test configurations.

In order to obtain the CCFL data in vertical-to-downwardly inclined pipes, Kawaji et al. [88,89] conducted countercurrent air–water experiments with six different test models containing elbows of varying angles. The inner diameter of the test sections was 51 mm, and the length of the vertical pipe was 1.0 m. They found that the formation of a hydraulic jump in the horizontal pipe near the bend has a significant effect on flooding in the vertical-to-horizontal pipe. They observed different CCFL mechanisms at various water flow rates in the vertical-to-horizontal pipe. For the test section with a long horizontal pipe (2.54 m), the hydraulic jump forms downstream of the bend and leads to flooding at low water flow rates ($J_L^{*1/2} < 0.4$); at moderate water flow rates ($0.4 < J_L^{*1/2} < 0.7$), the hydraulic jump develops away from the bend, and flooding occurs due to the slugging at the water exit; at high water flow rates ($J_L^{*1/2} > 0.8$), flooding takes place in the vertical pipe near the water entrance. For the test section with a short horizontal pipe (0.1 m), there are some differences in the flooding mechanisms. The flooding due to the formation of the hydraulic jump only occurs at the lowest water flow rate, i.e., $J_L^{*1/2} = 0.2$. For $0.2 < J_L^{*1/2} < 0.8$, the hydraulic jump is swept out of the short horizontal pipe, and flooding occurs due to the slugging in the horizontal pipe, which requires higher flooding gas velocity. For the CCFL mechanisms in the vertical-to-inclined pipe, they found that the flooding occurs due to slugging at low water flow rates and water droplets' entrainment/carryover at higher water flow rates. Compared with the vertical-to-horizontal pipe and vertical pipe, the flooding gas velocity in the vertical-to-inclined pipe is higher when $J_L^{*1/2} < 0.6$. They noticed that the effect of the bend angle on CCFL is small.

Ghiaasiaan et al. [90] carried out experimental investigations of CCFL using air and water in an inclined flow channel connected to elbows in both ends. It is noteworthy that no hysteresis phenomenon was observed between the flooding and deflooding data. This is because the "flooding data" and "deflooding data" in their studies actually comprise partial CCFL data, which are obtained by the experimental method with a constant water–head liquid injection. A Wallis-type correlation was correlated based on the CCFL data, and can be expressed as:

$$J_G^{*1/2} + 0.66 J_L^{*1/2} = 0.6 \tag{38}$$

Later, the countercurrent two-phase flow experiments using various working fluids were performed by Ghiaasiaan et al. in the same test facility to investigate the influences of liquid properties [91]. Results showed that the CCFL data for air–water and air–mineral oil are similar, and they are nearly independent of the inclination angle. The flooding gas velocity for air–paraffinic oil is much lower than that for air–water. In addition, the inclination angle has an effect on the flooding for air–paraffinic oil.

3.5. Flow Channel with Obstruction

Table 8 summarizes the experimental studies on two-phase countercurrent flow in the flow channel with obstruction. The test models in the experimental studies can be mainly divided into two categories, i.e., the model of PWR hot leg with Hutze [92,93] and the model of flow channel with an orifice or perforated plate [10,94–97].

A Hutze is a secondary pipe employed for hot leg emergency core cooling (ECC) injection and is installed in the horizontal section of the hot leg in some German PWRs. The Hutze may affect the CCFL characteristics in the PWR hot leg because the presence of a Hutze has an influence on the interface distribution by functioning as an obstacle to liquid flow. Wang and Mayinger [98] found that the Hutze brings about an appreciable

disturbance on the flow structure in the horizontal section. It is noteworthy that most downscaled experimental studies were performed without a Hutze. Issa [93] stated that the Hutze effect cannot be negligible. Ohnuki et al. [92] and Issa [93] carried out two-phase countercurrent flow experiments in PWR hot leg models to evaluate the Hutze effect.

Table 8. Summary of the experimental investigations on the CCFL in the flow channel with obstruction.

Authors	Test Fluids	Test Models	Inner Pipe Diameter (mm)	Remarks
Bankoff et al. [94] (1981)	Air–water, steam–water	Vertical rectangular channel with a horizontal perforated plate	Rectangular channel width: 71.5; rectangular channel height: 42.9	A CCFL correlation applied to flow channel with horizontal perforated plates in terms of a new scaling parameter was proposed
Ohnuki et al. [92] (1988)	Air–water, steam–water	PWR hot leg models with and without a Hutze	25.4	The presence of Hutze is considered to be one reason to lead to the discrepancy between the experimental data and the empirical correlations The Hutze effect becomes smaller with the decrease of the gas velocity
Celata et al. [10] (1989)	Air–water	Vertical pipe with obstruction	20, 16.2	A modified Wallis-type correlation based on the perforation ratio gives a good prediction The discrepancy between 20.0 mm and 16.2 mm diametesr data is very small The shape of the flow obstruction has a marginal effect on CCFL
Celata et al. [95] (1992)	Air–water	Vertical pipe with obstruction	20	The effect of a slight inclination from the vertical orientation on CCFL was investigated
Kawaji et al. [96] (1993)	Air–water	Flow channel with an orifice and multiple elbows	51	The presence of orifices lowers the flooding gas velocity, with the greatest effect for the smallest orifice tested The flooding gas velocity increases with the perforation ratio increases The flooding is simultaneously accompanied by the formation of slugs in the horizontal pipe
Teyssedou et al. [97] (2005)	Air–water	Flow channel with an orifice and two elbows	63.5	The flooding gas velocity decreases with increasing severity of the obstruction The onsets of flooding and slugging are independent of the position of the orifice
Issa [93] (2021)	Air–water	Model of 1/4 scale down of PWR hot leg with a Hutze	190	The Hutze effect on CCFL was studied Two Wallis-type correlations to represent the CCFL characteristics in the full-scale hot leg model without a Hutze were proposed

Ohnuki et al. [92] adopted two types of hot leg models in the experiments, that is, the hot leg models with and without a Hutze in the horizontal section. They found that $J_L^{*1/2}$ using nominal diameter for the hot leg model with a Hutze is smaller than without a Hutze at the same $J_G^{*1/2}$. The presence of a Hutze is considered to be one reason to lead to the discrepancy between the experimental data and the empirical correlations. The effect of a Hutze becomes smaller with the decrease of $J_G^{*1/2}$. The effect is eliminated by the modification of $J_K^{*1/2}$ using hydraulic diameter and area.

Recently, Issa [93] built a Hutze pipe into the hot leg model at COLLIDER test facility and compared the experimental results with the CCFL data in previous studies to investigate the Hutze effect on CCFL. The results indicated that the Hutze has a strong effect on CCFL data. The Hutze works as an obstacle for the falling water film, disturbing the liquid flow and creating an easier condition for the onset of hydraulic jumps. It also works like a dam after the jump occurrence, helping more water to be trapped behind the Hutze pipe. The presence of the Hutze restricts the gas flow area and less cooling water flows down to the RPV. For the hot leg model with a Hutze, two hydraulic jumps are observed before the occurrence of CCFL: one occurs in the Hutze region, and the other occurs at the bend. However, only one hydraulic jump takes place in the hot leg model without a Hutze. They found that the limits of the hydraulic jumps and CCFL occur at a much lower gas flow rate, and the hysteresis phenomenon disappears. Besides, they proposed two Wallis-type correlations to represent the CCFL characteristics in the full-scale hot leg model without a Hutze.

For the full-scale hot leg model without a Hutze, the correlation is expressed as:

$$J_G^{*1/2} + 1.17 J_L^{*1/2} = 0.7 \tag{39}$$

For the full-scale hot leg model without a Hutze excluding ZP, the correlation is expressed as:

$$J_G^{*1/2} + 0.76 J_L^{*1/2} = 0.66 \tag{40}$$

For some specific cases, the obstructions are installed in flow channels for flow adjustments or measurements in the nuclear power reactors [99]. Bankoff et al. [94] conducted air–water and steam–water countercurrent flows in a vertical rectangular channel with a horizontal perforated plate. They proposed a CCFL correlation applied to flow channels with horizontal perforated plates and to unheated full-length tube bundles with no mass transfer in terms of a new scaling parameter, and the correlation correlated a variety of CCFL data satisfactorily. For the cases with condensing mass transfer, the correlation can also be used to predict the onset of downward penetration or end-of-complete bypass by using the parameter of an effective dimensionless steam flow rate.

To study the effect of obstructions in flow channels, Celata et al. [10] performed air–water countercurrent experiments in a vertical circular pipe. The obstructions with different diameters were used in the experiments. The result indicated that the flooding gas velocity increases with the increase of the perforation ratio. They found that a modified Wallis-type correlation gives a good prediction; the correlation is described as:

$$J_G^{*1/2} + J_L^{*1/2} = \gamma^{0.35} \tag{41}$$

where is the perforation ratio, which is the fraction of the obstruction area occupied by the hole.

They carried out experiments with different channel diameters but with the same perforation ratio, and the discrepancy between 20.0 mm and 16.2 mm diameter data is very small. They also performed tests to evaluate the influence of multiple short paths on flooding data, the results indicated that the shape of the flow obstruction has a marginal effect on CCFL. Later, Celata et al. [95] investigated the effect of a slight inclination from the vertical orientation on CCFL in the same test facility. The results showed an initial increase in the flooding gas velocity for little deviation from the vertical orientation, which tends to reduce near 80°and become negligible for angles near 75°.

Kawaji et al. [96] performed experimental investigations on the air–water countercurrent flooding in complex flow channels with an orifice and multiple elbows. The results showed that the presence of an orifice lowers the flooding gas velocity, with the greatest effect for the smallest orifice tested. They noticed that a large orifice has very little influence on the CCFL. The flooding gas velocities for the small orifice and medium orifice are much smaller than those for large orifice and no orifice at a given liquid flow rate. Furthermore, the flooding gas velocity was found to increase with the increase of the perforation ratio, which is consistent with the conclusions of Tye [99] and Celata et al. [10].

To study the CCFL phenomena for vertical-to-horizontal countercurrent flows with an orifice installed in the horizontal pipe, Teyssedou et al. [97] performed countercurrent air–water flow experiments in the flow channels with an orifice and two elbows. It was observed that the flooding is simultaneously accompanied by the formation of slugs in the horizontal pipe in which an orifice is installed. The slugs occur due to the mutual interaction of two waves traveling in opposite directions. They suggested that the flooding gas velocity decreases with increasing the severity of the obstruction, and the onsets of flooding and slugging are independent of the position of the orifice.

4. Numerical Studies

With the development of CFD, it has become of interest to carry out numerical studies in nuclear reactor safety research over the past several decades. The CFD tool can simulate

most of the two-phase flow configurations encountered in nuclear power plants [100]. Compared with experimental investigations, numerical studies are more convenient and economical. In experiments, the CCFL characteristics are affected by various differences, such as specifications and characteristics of the test facility, test methods, test conditions, data measurement and evaluation methods, and so on. Therefore, it is of significance to verify numerical methods and confirm experimental results by the numerical calculations using the same computational model and scheme [101].

As shown in Table 9, many numerical studies have been performed to investigate the CCFL phenomena and mechanisms, flow patterns, and interface behaviors in gas–liquid countercurrent flow in a PWR. It can be seen that most researchers carried out numerical CCFL works in the PWR hot leg, especially Murase and his co-workers [101–110] and Höhne and his co-workers [100,111–113].

Wang and Mayinger [98] performed a 2D steady state numerical simulation for the two-phase flow. The interphase momentum transfer is represented by the interfacial friction model, created by using empirical correlations. For the boundary conditions of the hot leg model in the simulation, they set the inlet flow parameters to be constant and assumed that the outlet is fully developed. They reported that different flow structures appeared in the regions near and away from the CCFL curve under reflux condensation conditions. Wintterle et al. [114,115] carried out 2D transient simulations of air–water countercurrent flow in the horizontal rectangular channel simulating the test section of the WENKA test facility. A phase interaction model was derived. The numerical calculations for the supercritical flow conditions were in good conformity with the experimental results. They also noticed that the $k-\varepsilon$ turbulence model predicts the velocity and the turbulence level better for partially reversed flow than the $k-\omega$ model.

However, Murase and his co-workers stated that 2D simulations cannot account for the effects of wall friction correctly, and the boundary conditions should not be specified because the falling water flow rate through the hot leg is the output parameter of the simulation. Thus, they performed many 3D transient simulations on air–water and steam–water countercurrent flows in small-scale and full-scale models of a PWR hot leg to study the CCFL phenomenon [101–110]. The multi-fluid Euler–Euler approach was employed; some of the simulations adopted the two-fluid model, and some adopted the volume of fluid (VOF) model. They proposed that the two-fluid model gives a good agreement with the CCFL data under low pressure conditions, but shows more deviations under high pressure steam–water conditions. The VOF model agrees well with the CCFL data for rectangular channels but doesn't for circular channels.

Murase et al. [102,105] carried out CFD simulations in a 1/15 scale model of the PWR hot leg at Kobe University by using VOF model. The calculation domain includes the lower and the upper tank because the two-phase velocity distributions at the inlet and outlet of the hot leg would affect the hydraulic behaviors. In the simulation, a laminar flow model was employed, and the expansion of the inclined pipe was simulated, but the surface tension effect was not considered in the calculation. The simulation results showed that the flow pattern transition from stratified flow to wavy-mist flow cannot be calculated in the calculation without the expansion in the inclined pipe, whereas in the calculation with the expansion, the CCFL at the inclined pipe upper end is mitigated and the flow pattern transition is successfully simulated. By comparing the numerical results using VOF model with those using two-fluid model, they suggested that it is preferable to employ the two-fluid model with a suitable interface friction model, rather than the VOF model, to calculate global flow behaviors. They also compared the calculations using the standard $k-\varepsilon$ model and laminar model, it was shown that the numerical results using the standard $k-\varepsilon$ model greatly underestimate the falling water flow rates, but the results using laminar model agree well with the experimental data. They proposed that it is crucial to select the calculation models and conditions appropriately in the simulations.

Table 9. Summary of the numerical studies on CCFL.

Authors	CFD Code	Test Fluids	Test Geometry	Number of the Computational Grid	Multiphase Model	Viscous Model	Pressure-Velocity Coupling Scheme	Remarks
Wang and Mayinger [98] (1995)	FLOW3D	Steam–water	Model of full scale of a PWR hot leg	-	Stratified model	Standard $k-\varepsilon$	-	2D steady state simulation The hot leg inlet flow parameters were set to be constant and the fully developed assumption was applied to the outlet
Wintterle et al. [114,115] (2007, 2008)	ANSYS CFX 10	Air–water	Model of the test section of the WENKA test facility	-	Two-fluid model	$k-\omega$, $k-\varepsilon$	-	2D transient simulation A phase interaction model was derived The $k-\varepsilon$ turbulence model predicts the velocity and the turbulence level better for partially reversed flow than the $k-\omega$ model
Murase et al. [102] (2009)	FLUENT6.3.26	Air–water	Model of 1/15 scale of a PWR hot leg	70,000	VOF	Laminar	Phase-coupled SIMPLE	3D transient simulation The effect of the expansion of the inclined pipe was evaluated It is preferable to employ the two-fluid model with a suitable interface friction model rather than the VOF model to calculate global flow behaviors
Minami et al. [103] (2010)	FLUENT6.3.26	Air–water	Model of 1/15 scale of a PWR hot leg	70,000	Two-fluid model	Standard $k-\varepsilon$	Phase-coupled SIMPLE	3D transient simulation A combination of the interfacial friction coefficient correlations was applied The proposed model fails to predict the formation of small waves in wavy flows
Kinoshita et al. [104] (2010)	FLUENT6.3.26	Air–water, steam–water	Models of 1/15 scale and full scale of a PWR hot leg	70,000	Two-fluid model	Standard $k-\varepsilon$	Phase-coupled SIMPLE	3D transient simulation The effect of the expansion of the inclined pipe was examined A Wallis-type correlation was correlated, and the correlation is applicable in the pipe diameter range of 0.05 m ~ 0.75 m
Murase et al. [105] (2012a)	FLUENT6.3.26	Air–water	Models of 1/15 scale and full scale of a PWR hot leg	59,000	VOF	Laminar, Standard $k-\varepsilon$	PISO	3D transient simulation The effect of the turbulence model was studied The computational grids in the domain of the hot leg and the computational scheme in the simulations were improved
Murase et al. [106] (2012b)	FLUENT6.3.26	Steam–water	Model of full scale of a PWR hot leg	59,000	VOF	Standard $k-\varepsilon$	PISO	3D transient simulation The simulation results were in excellent agreement with the UPTF data at 1.5 MPa except for at high gas flow rates
Murase et al. [107] (2012c)	FLUENT6.3.26	Steam–water	Model of full scale of a PWR hot leg	59,000	VOF	Standard $k-\varepsilon$	PISO	3D transient simulation The CCFL characteristics are independent of the gas density but affected by the liquid viscosity
Utanohara et al. [108] (2011)	FLUENT6.3.26	Air–water, steam–water	Models of 1/15 scale and full scale of a PWR hot leg	70,000, 120,000	Two-fluid model	Standard $k-\varepsilon$	Phase-coupled SIMPLE	3D transient simulation The cell size affects the flooding gas velocity in the process of increasing gas flow rate
Utanohara et al. [109] (2012)	FLUENT6.3.26	Steam–water	1/3 scale of hot leg model with rectangular cross-section	136,000	VOF, two-fluid model	Standard $k-\varepsilon$	Phase-coupled SIMPLE	3D transient simulation The effects of the multiphase model and the fluid properties on CCFL were investigated The CCFL characteristics are affected by gas density and liquid viscosity
Kinoshita et al. [110] (2012)	FLUENT6.3.26	Air–water	Model of 1/30 scale of a PWR hot leg	120,000	Two-fluid model	Standard $k-\varepsilon$	Phase-coupled SIMPLE	3D transient simulation The size effect was investigated
Kinoshita et al. [101] (2014)	FLUENT6.3.26	Air–water	1/3 scale of hot leg model with rectangular cross-section	136,000	VOF, two-fluid model	Standard $k-\varepsilon$	Phase-coupled SIMPLE	3D transient simulation The effects of flow channel shape and size, and the multiphase model were evaluated
Höhne et al. [112] (2011)	ANSYS CFX 12.1	Air–water, steam–water	1/3 scale of hot leg model with rectangular cross-section	248,610	Two-fluid model	SST	-	3D transient simulation The AIAD model was applied The numerical results were in a good agreement with the experimental data.
Deendarlianto et al. [100] (2011)	ANSYS CFX 12.0	Air–water, steam–water	1/3 scale of hot leg model with rectangular cross-section	248,610	Two-fluid model	SST	-	3D transient simulation The AIAD model was applied The numerical results were in a good agreement with the experimental data.
Höhne and Deendarlianto [112] (2012)	ANSYS CFX 12.0	Steam–water	Model of full scale of a PWR hot leg	-	Two-fluid model	SST	-	3D transient simulation The AIAD model was applied The simulation results agreed well with the experimental data
Porombka and Höhne [113] (2015)	ANSYS CFX 14.5	Air–water	Model of the test section of the WENKA facility	526,000 nodes	Two-fluid model	$k-\omega$	-	3D transient simulation The AIAD model was revised and a modified free surface drag model and morphology detection mechanism were proposed The turbulence dampening was found to be crucial for the $k-\omega$ turbulence model
Issa and Juan [116] (2016)	ANSYS CFX 14.5	Air–water	Model of 1/3.9 scale of a PWR hot leg	203,503	Two-fluid model	SST	-	3D transient simulation The simulation results were in excellent agreement with the experiments regarding the onset of bend-CCFL The numerical approach cannot predict the onset of ADE-CCFL
Watanabe et al. [117] (2017)	-	Air–water	Model of a vertical channel	-	VOF	-	SMAC	2D transient simulation The coupled VOF method was applied
Samal and Ghosh [118] (2020)	-	Air–water	1/3 scale of hot leg model with rectangular cross-section	-	VOF	$k-\omega$	PISO	2D transient simulation The flow-structures were characterized and parameterized in terms of the statistical parameters.

Later, Minami et al. [103] and Kinoshita et al. [104] performed the simulations in the 1/15 scale model of the PWR hot leg using the two-fluid model. Note that a combination of the interfacial friction coefficient correlations was applied to calculate the interfacial friction force in the momentum equation, and is given by:

$$\begin{gathered} C_D A_i = min[(C_D A_i)_B, max\{(C_D A_i)_S, (C_D A_i)_A\}] \\ (C_D A_i)_B = \frac{2\alpha(1-\alpha)g}{V_{gj}^2} \\ (C_D A_i)_S = 9.8(1-\alpha)^3 \frac{4.5\alpha}{D} \\ (C_D A_i)_A = 0.02\alpha^{0.5} \frac{1+75(1-\alpha)}{D} \end{gathered} \tag{42}$$

where A_i is the interfacial area concentration, $C_D A_i$ is the interfacial friction coefficient, α is the void fraction, V_{gj} is the drift velocity of the gas phase, and is given by:

$$V_{gj} = 1.4 D^{*0.125} \left\{ \frac{g\sigma(\rho_L - \rho_G)}{\rho_L^2} \right\}^{1/4} \tag{43}$$

It was found that the CCFL characteristics and flow patterns agree well with the experimental data. Minami et al. also reproduced the hysteresis phenomenon in the flow pattern. They reported that the selected combination of the correlations for interfacial friction coefficients can be utilized for the 3D two-fluid simulation of countercurrent two-phase flows in a hot leg geometry. However, the proposed model fails to predict the formation of small waves in wavy flows. Kinoshita et al. also examined the effect of the expansion of the inclined pipe. They found that when the expansion exists, the CCFL at the upper end of the inclined pipe doesn't occur, and the flow pattern transition from stratified flow to wavy-mist flow takes place at higher gas flow rates.

Numerical simulations of gas–liquid countercurrent flow in the full-scale model of a PWR hot leg were also conducted by Kinoshita et al. [104] and Murase et al. [105–107]. Kinoshita et al. [104] performed simulations of a full-scale hot leg model at 0.1 MPa for air-water flow and at 0.1, 0.3 MPa for steam–water flow by using a two-fluid model. A Wallis-type correlation was correlated for the prediction of CCFL characteristics in the hot leg model, and they confirmed that the correlation is applicable in the pipe diameter range of 0.05 m ~ 0.75 m. Murase et al. [105] conducted simulations for full-scale air–water conditions at 0.1 MPa using the VOF method. They improved the computational grids in the domain of the hot leg and the computational scheme in the simulations. The numerical results showed a satisfactory agreement with experimental data. Next, Murase et al. [106] carried out steam–water simulations at 1.5 MPa under the full-scale conditions using the same numerical models. The simulation results indicated that the calculated CCFL characteristics are in excellent agreement with the UPTF data at 1.5 MPa except for at high gas flow rates. In order to study the effects of system pressure and fluid properties on CCFL in the hot leg model, steam–water simulations for system pressures up to 8 MPa under the full-scale conditions were conducted by Murase et al. [107]. They reported that the CCFL characteristics are independent of the gas density but affected by the liquid viscosity. When the system pressure is below 1.5 MPa, the constant C in the Wallis-type correlation increases with the increase of system pressure, and C becomes almost constant when the system is greater than 1.5 MPa.

It was reported that the parameters of main concern in the numerical studies were the multiphase model, the flow channel size, cell size, and fluid properties. To evaluate the effects of the interfacial drag correlations and the cell size on CCFL characteristics, Utanohara et al. [108] carried out simulations of countercurrent gas–liquid flow in the 1/15 scale and full scale hot leg models. The numerical results showed that the cell size affects the flooding gas velocity in the process of increasing gas flow rate, and the flooding gas velocity obtained by using fine cells is higher than that by using normal cells. However, the CCFL characteristics are independent of the cell size in the process of decreasing gas flow rate. In the simulations, different interfacial friction coefficient correlations presented

by Minami et al. [103] were used to investigate the effect of the interfacial drag coefficient. It was found that the reference interfacial drag correlations can be applied to the PWR conditions. Later, Utanohara et al. [109] performed simulations for steam–water CCFL tests in the 1/3 scale rectangular channel simulating a PWR hot leg. The objective of the work was to examine the effects of the multiphase model and the fluid properties on CCFL. They reported that The CCFL characteristics predicted by the VOF method and two-fluid model agree well with the CCFL data, and the CCFL is mitigated at high pressure conditions. However, both simulations using the two models underestimate the slope of the CCFL curve and overestimate the effects of fluid properties on CCFL characteristics. In addition, the simulation using the VOF method shows a better prediction ability for fluid properties than the two-fluid simulations. They also proposed that the CCFL characteristics are affected by gas density and liquid viscosity.

Kinoshita et al. [101,110] evaluated the effects of flow channel shape and size, and the multiphase model. The test geometries in their simulations were the 1/30 scale hot leg model with the diameter of 25.4 mm, and the 1/3 scale hot leg model with a rectangular channel. They employed the same numerical methods in their previous works for the simulations. They observed that the constant C in Wallis-type correlation becomes small for the small-diameter simulation, and the CCFL difference between $D = 25.4$ mm and 25.4 mm $\leq D \leq$ 750 mm is caused by a size effect and not by other factors. They suggested that the CCFL characteristics are independent of the location of gas inlet, and that the constant C is affected by the aspect ratio and size in the rectangular channel. The flow patterns predicted by the two-fluid model and the VOF method are shown in Figures 17 and 18, respectively. They reported that the simulations using the two-fluid model with the proposed set of interfacial drag coefficient correlations can evaluate the effects of channel shape and size on the CCFL constants, and the simulations using the VOF method reproduce the trend of the effects but underestimate the CCFL constants.

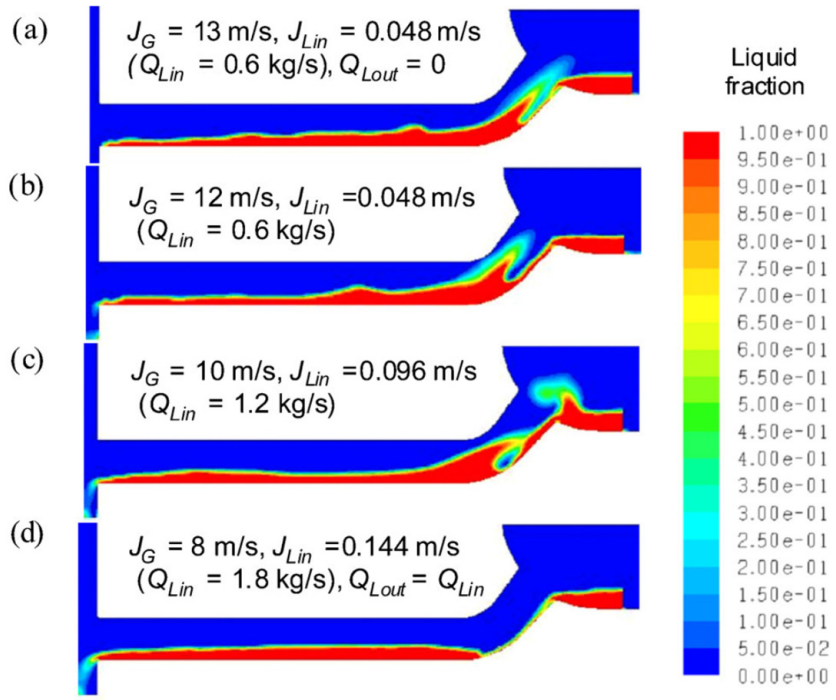

Figure 17. Flow patterns predicted by the two-fluid model (0.15 MPa); (**a**–**d**) flow patterns for different simulation cases (Kinoshita et al. [101]).

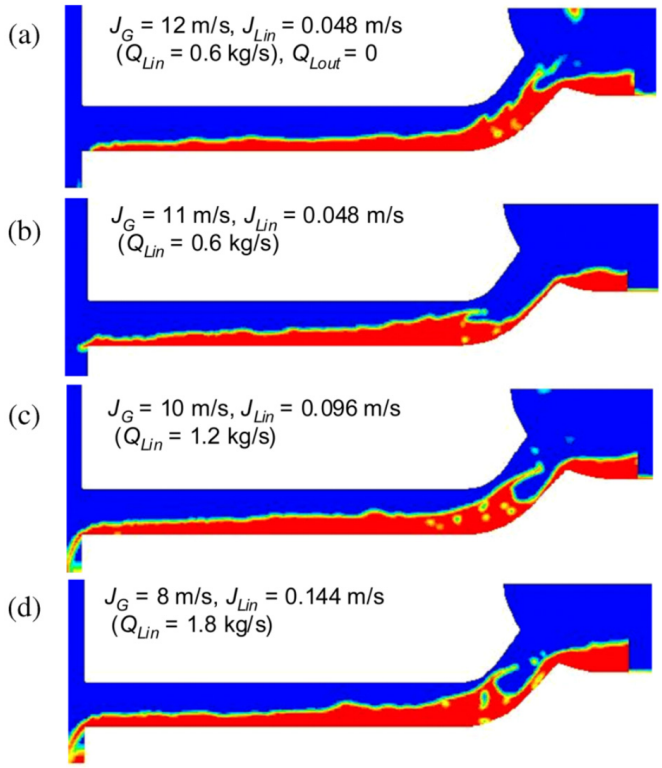

Figure 18. Flow patterns predicted by the VOF method (0.15 MPa); (**a**–**d**) flow patterns for different simulation cases (Kinoshita et al. [101]).

Höhne and his co-workers also carried out a series of numerical studies on gas–liquid countercurrent flow in the PWR hot leg model [100,111–113]. In the simulations, the two-fluid model was implemented. The interfacial drag was approached by a new correlation inside the algebraic interfacial area density (AIAD) model based on the implemented mixture model [119]. Höhne et al. [111] and Deendarlianto et al. [100] conducted 3D transient simulations of the 1/3 scale German Konvoi PWR hot leg model with a rectangular cross-section. Air–water and steam–water were employed as test fluids in the simulations, and the two-fluid model coupled with shear stress transport (SST) turbulence model was implemented. It was found that the simulation can reproduce the basic flow characteristics such as the hydraulic jump near the elbow and the onset of roll waves, which were observed in the experiment. Figure 19 shows the flow structure of the steam–water counter-current flow near the elbow around flooding. Furthermore, the calculated CCFL characteristics give a quantitative agreement with the experimental data.

In order to validate the AIAD model and to evaluate the scaling effects on CCFL, Höhne and Deendarlianto [112] carried out numerical simulations of the CCFL phenomenon in a full scale PWR hot leg model. The result indicated that the simulation results agree well with the experimental data. It is noteworthy that the applicability of the drag model is limited to certain flow regimes because the drag models are often based on experimental correlations. To avoid this limitation, Porombka and Höhne [113] revised the AIAD model and proposed a modified drag model and morphology detection mechanism. They conducted numerical simulations of stratified countercurrent air–water flow in the model of the complete test section of the WENKA facility using the two-fluid model coupled with the modified AIAD model. Satisfactory CFD results were obtained in the simulations. In addition, the turbulence dampening was found to be crucial for the $k-\omega$ turbulence model.

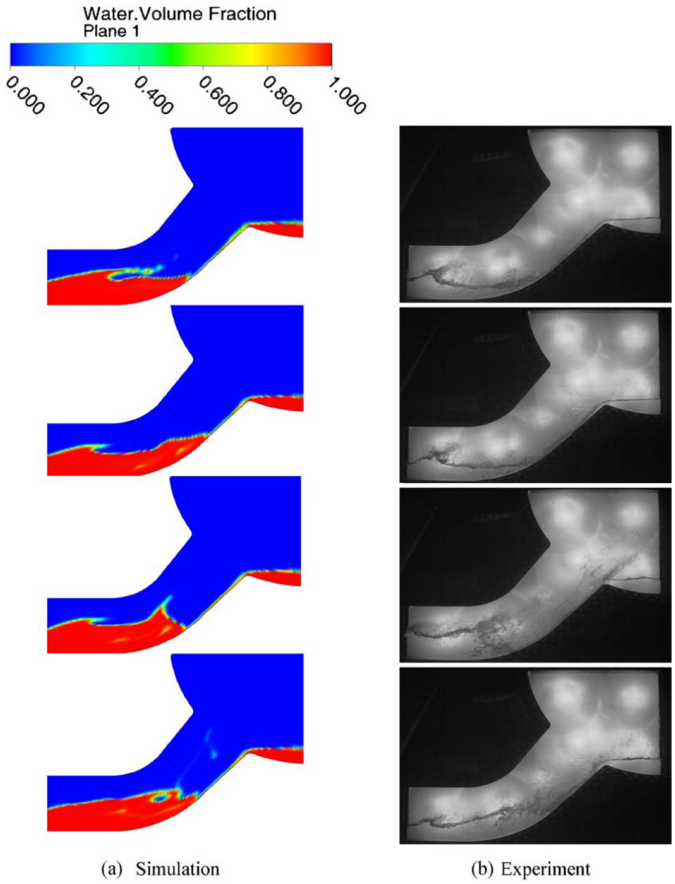

Figure 19. Flow structure of the steam–water counter-current flow near the elbow around flooding (Q_G = 0.530 kg/s); (**a**) calculated water volume fraction and (**b**) visual observation obtained from experiment (Deendarlianto et al. [100]).

Issa and Juan [116] performed 3D CFD simulations of air–water countercurrent in the 1/3.9 scale of a PWR hot leg geometry. The two-fluid model with a free-surface approach and an interfacial drag coefficient model presented by Minami et al. [103] were implemented in the simulations. A water inlet with constant velocity and an air inlet with a time function were employed. The CFL results were in excellent agreement with the experiments regarding the onset of bend-CCFL, the onset of the jump was well predicted, and the water depth distribution in the simulation agreed well with that in the experiment. Unfortunately, the numerical approach used in their studies cannot predict the onset of ADE-CCFL. To investigate the flow conditions and flow structures in the hot leg geometry, Samal and Ghosh [118] carried out 2D transient simulations of countercurrent air–water flow in the 1/3 scale of the German Konvoi PWR hot leg model with a rectangular cross-section. They employed the VOF method and the k − ω turbulence model in the simulations. They extracted statistical parameters from the time variation of pressure drop and volume fraction across the flow domain, and the flow-structures in the hot leg were characterized and parameterized in terms of the statistical parameters.

Watanabe et al. [117] modified the existing 1D liquid film flow model and designed the flow network of virtual liquid film and coupled it with the VOF method. Based on the coupled VOF method, they conducted 2D simulations of air-water countercurrent flow in a vertical channel, and the channel width is 0.02 m. They noticed that there seems to be no significant difference in the CCFL characteristics between the only VOF method and the coupled VOF method with regard to the total falling liquid flow rate, but the liquid downward volumetric flux can be evaluated using the coupled VOF method. Chen and Zhang [120] developed a transient analysis code based on a 1D, six-equation, two-fluid model to describe the two-phase countercurrent flow. They suggested that mesh

size significantly affects the simulated results. Riva and Col [121] and Tekavcic et al. [122] investigated the countercurrent gas–liquid countercurrent churn flow in the vertical channel. Also, some numerical simulations of gas–liquid co-current flow were carried out to study the two-phase flow phenomena [123–127].

5. Discussion

As can be seen from the previous sections, most researchers conducted countercurrent flow experiments using air and water at ambient pressure, and relatively fewer investigations using steam–water under high system pressure were carried out due to the limitation of the test facilities and test conditions. The CCFL in real PWR conditions is more complex, which relates to heat and mass transfer. Thus, the applicability of the obtained CCFL characteristics to real PWR conditions is questionable. It is necessary to develop advanced experimental techniques and image processing to provide a further understanding of CCFL. Additionally, high quality experimental data are required to recognize the detailed flow phenomena and the gas–liquid interface structures and to provide validations of the CFD models.

A large number of numerical studies for countercurrent two-phase flow in a PWR hot leg geometry have been performed, but the simulations in other flow channels were relatively rare. Additionally, most of the numerical simulations do not include heat and mass transfer. Therefore, it is necessary to investigate the effects of heat and mass transfer experimentally and numerically. Furthermore, most 3D simulations for countercurrent two-phase flow fail to predict the formation of small waves and the details in two-phase flow. This is mainly because the computational grid used for calculation is not fine enough. It is of significance to perform numerical simulations for countercurrent two-phase flow with a fine computational grid and suitable model.

In addition, the CCFL empirical correlations need to be embedded into complex computer codes to calculate the major parameters such as void fraction and pressure drops for safety evaluations of nuclear reactors. The quality-judgement for the calculation models may be affected by the calculated parameters and the application to nuclear reactor accident analysis for specific geometry.

6. Conclusions

In this paper, we performed a comprehensive review of the studies on two-phase countercurrent flow limitation in a PWR, including the experimental investigations and the numerical studies. The experimental investigations of CCFL phenomena in a PWR were reviewed in terms of the flow channel geometry. Additionally, many of numerical studies for countercurrent two-phase flow were carried out with the development of CFD. Different numerical models were presented and applied to predict the CCFL phenomenon in the test geometry. Through the comprehensive review, the following conclusions are obtained:

(1). The CCFL is significantly affected by geometrical characteristics, including the geometrical size, the channel shape, the channel orientation, and the channel with or without obstruction. The CCFL mechanisms and CCFL characteristics may be different for the flow channels with different geometrical characteristics.

(2). The fluid properties and condensation have effects on CCFL. Numerous investigations with various combinations of fluids and under different system pressures have been carried out to study the effects of fluid properties on CCFL. It was found that the surface tension, the liquid viscosity, and the liquid density affect the CCFL, but the effect of gas density is not clear enough.

(3). The "CCFL data" term was widely used in the literature. CCFL data refer to the data of the onset of flooding and partial CCFL data. The data of the onset of flooding differ from the deflooding data and partial CCFL data. They should be carefully used to avoid ambiguity.

(4). Many numerical models were presented and modified to predict the two-phase flow patterns and the CCFL characteristics in the test channel. The VOF method and the

two-fluid model are the two frequently used multiphase models in numerical studies. Both the two multiphase models have advantages and disadvantages; it is important to choose the suitable model in the numerical simulation. The interfacial drag coefficient model is also of significance to the numerical calculation when applying the two-fluid model.

Author Contributions: Conceptualization, X.Z. and N.W.; methodology, X.Z., Z.W. and C.X.; validation, X.Z., Z.W. and C.X.; formal analysis, X.Z. and N.W.; investigation, X.Z., Z.W. and C.X.; writing—original draft preparation, X.Z. and N.W.; writing—review and editing, X.Z., Z.W., C.X. and N.W.; supervision, N.W.; project administration, N.W. All authors have read and agreed to the published version of the manuscript.

Funding: This research received no external funding.

Data Availability Statement: Not applicable.

Conflicts of Interest: The authors declare no conflict of interest.

Nomenclature

General Symbols	
a	vertical rectangular channel width, m
b	vertical rectangular channel gap, m
Bo	bond number
C	constant
D	inner diameter of pipe, m
Fr	Froude number
g	acceleration of gravity, m/s^2
h	water level
H	rectangular channel height, m
J	superficial velocity, m/s
Ku	Kutateladze number
L	channel length, m
m	constant
Q	mass flow rate, kg/s
V	velocity, m/s
W	rectangular channel width, m
X	dimensionless parameter
Y	dimensionless parameter
Greek alphabet	
α	void friction
γ	perforation ratio
θ	inclination angle, $^\circ$
μ	viscosity, Pa·s
ρ	density, kg/m^3
σ	surface tension, N/m
Superscript	
*	dimensionless
Subscripts	
D	drag
eq	equivalent
gj	drift velocity of gas phase
G	gas
H	horizontal section of the hot leg
HL	hot leg
in	inlet
I	inclined section of the hot leg
K	gas/liquid
L	liquid

Abbreviations

1D	one-dimensional
2D	two-dimensional
3D	three-dimensional
ADE	active droplets entrainment
ADS	automatic depressurization system
AIAD	algebraic interfacial area density
CCF	countercurrent flow
CCFL	countercurrent flow limitation
CFD	computational fluid dynamics
COLLIDER	countercurrent limitation in a large diameter geometry
ECC	emergency core coolant
ECCS	emergency core coolant system
LOCA	loss of coolant accident
PWR	pressurized water reactor
RPV	reactor pressure vessel
SBLOCA	small break loss of coolant accident
SG	steam generator
SST	shear stress transport
TOPFLOW	transient two phase flow
UPTF	upper plenum test facility
VOF	volume of fluid
ZP	zero liquid penetration

References

1. Deendarlianto; Vallée, C.; Lucas, D.; Beyer, M.; Pietruske, H.; Carl, H. Experimental Study on the Air/Water Counter-Current Flow Limitation in a Model of the Hot Leg of a Pressurized Water Reactor. *Nucl. Eng. Des.* **2008**, *238*, 3389–3402, Erratum in *Nucl. Eng. Des.* **2011**, *241*, 3359–3372. [CrossRef]
2. Navarro, M.A. Study of Countercurrent Flow Limitation in a Horizontal Pipe Connected to an Inclined One. *Nucl. Eng. Des.* **2005**, *235*, 1139–1148. [CrossRef]
3. Deendarlianto; Höhne, T.; Murase, M. Countercurrent Flow Limitations in a Pressurized Water Reactor. *Sci. Technol. Nucl. Install.* **2012**, *2012*, 608678. [CrossRef]
4. Yu, J.; Zhang, D.; Shi, L.; Wang, Z.; Yan, S.; Dong, B.; Tian, W.; Su, G.H.; Qiu, S. Experimental Investigation of Air-Water CCFL in the Pressurizer Surge Line of AP1000. *Nucl. Technol.* **2016**, *196*, 614–640. [CrossRef]
5. Wallis, G.B. Flooding Velocities for Air and Water in Vertical Tubes. In *UKAEA Report, AAEW-R 123*; United Kingdom Atomic Energy Authority: Dorset, UK, 1961.
6. Bankoff, S.G.; Lee, S.C. A Critical Review of the Flooding Literature. In *Proceedings of the NUREG/CR-3060*; U.S. Nuclear Regulatory Commission: Washington, DC, USA, 1983.
7. Al Issa, S.; Macian, R. A Review of CCFL Phenomenon. *Ann. Nucl. Energy* **2011**, *38*, 1795–1819. [CrossRef]
8. Deendarlianto; Höhne, T.; Lucas, D.; Vierow, K. Gas-Liquid Countercurrent Two-Phase Flow in a PWR Hot Leg: A Comprehensive Research Review. *Nucl. Eng. Des.* **2012**, *243*, 214–233. [CrossRef]
9. Morghi, Y.; Zacarias Mesquita, A.; Puente, J.; Rosa Baliza, A. Investigation of Counter-Current Flow Limitation for Air-Water in a Pwr Hot Leg Experimental Loop for Different Geometry. *Int. J. Eng. Technol. Manag. Res.* **2018**, *5*, 198–212. [CrossRef]
10. Celata, G.P.; Cumo, N.; Farello, G.E.; Setaro, T. The Influence of Flow Obstructions on the Flooding Phenomenon in Vertical Channels. *Int. J. Multiph. Flow* **1989**, *15*, 227–239. [CrossRef]
11. Kang, S.K.; Chu, I.C.; No, H.C.; Chun, M.H. Air–Water Countercurrent Flow Limitation in a Horizontal Pipe Connected to an Inclined Riser. *J. Korean Nucl. Soc.* **1999**, *31*, 548–560.
12. Wallis, G.B.; Makkenchery, S. The Hanging Film Phenomenon in Vertical Annular Two-Phase Flow. *J. Fluids Eng.* **1974**, *96*, 297–298. [CrossRef]
13. Pushkina, O.L.; Sorokin, Y.L. Breakdown of Liquid Film Motion in Vertical Tubes. *Heat Transf. Sov Res* **1969**, *1*, 56–64.
14. Chung, S.K.; Liu, L.P.; Tien, C.L. Flooding in Two-Phase Countercurrent Flows.II. Experimental Investigation. *Physieoehem. Hydrodyn* **1980**, *1*, 209–220.
15. Mcquillan, K.W.; Whalley, P.B.; Hewitt, G.F. Flooding in Vertical Two-Phase Flow. *Int. J. Multiph. Flow* **1985**, *11*, 741–760. [CrossRef]
16. Suzuki, S.; Ueda, T. Behaviour of Liquid Films and Flooding in Counter-Current Two-Phase Flow—Part 1. Flow in Circular Tubes. *Int. J. Multiph. Flow* **1977**, *3*, 517–532. [CrossRef]
17. Osakabe, M.; Kawasaki, Y. Top Flooding in Thin Rectangular and Annular Passages. *Int. J. Multiph. Flow* **1989**, *15*, 747–754. [CrossRef]

18. Sudo, Y.; Usui, T.; Kaminaga, M. Experimental Study of Falling Water Limitation under a Counter-Current Flow in a Vertical Rectangular Channel: 1st Report, Effect of Flow Channel Configuration and Introduction of CCFL Correlation. *JSME Int. J. Ser. 2 Fluids Eng. Heat Transf. Power Combust. Thermophys. Prop.* **1991**, *34*, 169–174. [CrossRef]
19. Vijayan, M.; Jayanti, S.; Balakrishnan, A.R. Effect of Tube Diameter on Flooding. *Int. J. Multiph. Flow* **2001**, *27*, 797–816. [CrossRef]
20. Drosos, E.I.P.; Paras, S.V.; Karabelas, A.J. Counter-Current Gas-Liquid Flow in a Vertical Narrow Channel-Liquid Film Characteristics and Flooding Phenomena. *Int. J. Multiph. Flow* **2006**, *32*, 51–81. [CrossRef]
21. Matsumura, K.; Kaminaga, F. Experimental Investigation of Rising Gas Bubble Characteristics from a Vertical Tube under CCFL Condition. *Sci. Technol. Nucl. Install.* **2012**, *2012*, 785157. [CrossRef]
22. Doi, T.; Futatsugi, T.; Murase, M.; Hayashi, K.; Hosokawa, S.; Tomiyama, A. Countercurrent Flow Limitation at the Junction between the Surge Line and the Pressurizer of a PWR. *Sci. Technol. Nucl. Install.* **2012**, *2012*, 754724. [CrossRef]
23. Kusunoki, T.; Murase, M.; Fujii, Y.; Nozue, T.; Hayashi, K.; Hosokawa, S.; Tomiyama, A. Effects of Fluid Properties on CCFL Characteristics at a Vertical Pipe Lower End. *J. Nucl. Sci. Technol.* **2015**, *52*, 887–896. [CrossRef]
24. Wan, J.; Sun, W.; Deng, J.; Pan, L.; Ding, S. Experimental Study on Air-Water Countercurrent Flow Limitation in a Vertical Tube Based on Measurement of Film Thickness Behavior. *Nucl. Eng. Technol.* **2021**, *53*, 1821–1833. [CrossRef]
25. Ma, Y.; Zeng, S.; Shao, J.; Zhou, T.; Lyu, J.; Li, J.; Lu, P. An Experimental Study on Gas–Liquid Two-Phase Countercurrent Flow Limitations of Vertical Pipes. *Exp. Therm. Fluid Sci.* **2023**, *141*, 110789. [CrossRef]
26. Ueda, T.; Suzuki, S. Behaviour of Liquid Films and Flooding in Counter-Current Two-Phase Flow—Part 2. Flow in Annuli and Rod Bundles. *Int. J. Multiph. Flow* **1978**, *4*, 157–170. [CrossRef]
27. Asali, J.C.; Hanratty, T.J.; Andreussi, P. Interfacial Drag and Film Height for Vertical Annular Flow. *AIChE J.* **1985**, *31*, 895–902. [CrossRef]
28. Fukano, T.; Furukawa, T. Prediction of the Effects of Liquid Viscosity on Interfacial Shear Stress and Frictional Pressure Drop in Vertical Upward Gas-Liquid Annular Flow. *Int. J. Multiph. Flow* **1998**, *24*, 587–603. [CrossRef]
29. Belt, R.J.; Van't Westende, J.M.C.; Portela, L.M. Prediction of the Interfacial Shear-Stress in Vertical Annular Flow. *Int. J. Multiph. Flow* **2009**, *35*, 689–697. [CrossRef]
30. Goda, R.; Hayashi, K.; Murase, M.; Hosokawa, S.; Tomiyama, A. Experimental Study on Interfacial and Wall Friction Factors under Counter-Current Flow Limitation in Vertical Pipes with Sharp-Edged Lower Ends. *Nucl. Eng. Des.* **2019**, *353*, 110223. [CrossRef]
31. Goda, R.; Kurimoto, R.; Hayashi, K.; Murase, M.; Tomiyama, A. Effects of Fluid Properties on Interfacial and Wall Friction Factors under Counter-Current Flow Limitation in a Vertical Pipe with Sharp-Edged Lower End. *Nucl. Eng. Des.* **2021**, *373*, 111020. [CrossRef]
32. Takaki, T.; Murase, M.; Nishida, K.; Goda, R.; Shimamura, T.; Tomiyama, A. Liquid Film Thickness in Vertical Circular Pipes Under Flooding Conditions at the Top End. *Nucl. Technol.* **2020**, *206*, 389–400. [CrossRef]
33. Wallis, G.B.; Dodson, J.E. The Onset of Slugging in Horizontal Stratified Air-Water Flow. *Int. J. Multiph. Flow* **1973**, *1*, 173–193. [CrossRef]
34. Gardner, G.C. Flooded Countercurrent Two-Phase Flow in Horizontal Tubes and Channels. *Int. J. Multiph. Flow* **1982**, *9*, 367–382. [CrossRef]
35. Bankoff, S.G.; Lee, S.C. Flooding and Hysteresis Effects in Nearly-Horizontal Countercurrent Stratified Steam-Water Flow. *Int. J. Heat Mass Transf.* **1987**, *30*, 581–588. [CrossRef]
36. Ansari, M.R.; Nariai, H. Experimental Investigation on Wave Initiation and Slugging of Air-Water Stratified Flow in Horizontal Duct. *J. Nucl. Sci. Technol.* **1989**, *26*, 681–688. [CrossRef]
37. Wang, H.; Kondo, S. A Study on the Stratified Horizontal Counter-Current Two-Phase Flow. *Nucl. Eng. Des.* **1990**, *121*, 45–52. [CrossRef]
38. Choi, K.Y.; No, H.C. Experimental Studies of Flooding in Nearly Horizontal Pipes. *Int. J. Multiph. Flows* **1995**, *21*, 419–436. [CrossRef]
39. Chun, M.H.; Yu, S.O. A Theoretical and Experimental Study of the Steam Condensation Effect on the CCFL in Nearly Horizontal Two-Phase Flow. *J. Korean Nucl. Soc.* **1999**, *31*, 618–630.
40. Chun, M.H.; Yu, S.O. Effect of Steam Condensation on Countercurrent Flow Limiting in Nearly Horizontal Two-Phase Flow. *Nucl. Eng. Des.* **2000**, *196*, 201–217. [CrossRef]
41. Gargallo, M.; Schulenberg, T.; Meyer, L.; Laurien, E. Counter-Current Flow Limitations during Hot Leg Injection in Pressurized Water Reactors. *Nucl. Eng. Des.* **2005**, *235*, 785–804. [CrossRef]
42. Ma, Y.; Shao, J.; Lyu, J.; Peng, J. Experimental Study on the Effect of Diameter on Gas–Liquid CCFL Characteristics of Horizontal Circular Pipes. *Nucl. Eng. Des.* **2020**, *364*, 110645. [CrossRef]
43. Dhar, M.; Ray, S.; Das, G.; Kumar Das, P. Hydraulic Jump Induced Flooding and Slugging in Stratified Gas-Liquid Flow—An Experimental Appraisal. *Exp. Therm. Fluid Sci.* **2022**, *134*, 110617. [CrossRef]
44. Lee, S.C.; Bankoff, S.G. Stability of Steam-Water Countercurrent Flow in an Inclined Channel. *J. Heat Transfer* **1983**, *105*, 713–718. [CrossRef]
45. Barnea, D.; Yoseph, N.B.; Taitel, Y. Flooding in Inclined Pipes—Effect of Entrance Section. *Can. J. Chem. Eng.* **1986**, *64*, 177–184. [CrossRef]

46. Wongwises, S. Effect of Inclination Angles and Upper End Conditions on the Countercurrent Flow Limitation in Straight Circular Pipes. *Int. Commun. Heat Mass Transf.* **1998**, *25*, 117–125. [CrossRef]
47. Zapke, A.; Kröger, D.G. Countercurrent Gas-Liquid Flow in Inclined and Vertical Ducts—I: Flow Patterns, Pressure Drop Characteristics and Flooding. *Int. J. Multiph. Flow* **2000**, *26*, 1439–1455. [CrossRef]
48. Deendarlianto; Ousaka, A.; Indarto; Kariyasaki, A.; Lucas, D.; Vierow, K.; Vallee, C.; Hogan, K. The Effects of Surface Tension on Flooding in Counter-Current Two-Phase Flow in an Inclined Tube. *Exp. Therm. Fluid Sci.* **2010**, *34*, 813–826. [CrossRef]
49. Prayitno, S.; Santoso, R.A.; Deendarlianto; Höhne, T.; Lucas, D. Counter Current Flow Limitation of Gas-Liquid Two-Phase Flow in Nearly Horizontal Pipe. *Sci. Technol. Nucl. Install.* **2012**, *2012*, 513809. [CrossRef]
50. Siddiqui, H.; Baanderjee, S.; Ardron, K.H. Flooding in a N Elbow Between a Vertical a N D a Horizontal or Near-Horizontal Pipe. *Int. J. Multiph. Flow* **1986**, *12*, 531–541. [CrossRef]
51. Wan, P.T.; Krishnan, V.S. Air–Water Flooding in a 90° Elbow with a Slightly Inclined Lower Leg. In Proceedings of the Seventh Annual Conference of the Canadian Nuclear Society, Toronto, ON, Canada, 9–10 June 1986; pp. 273–278.
52. Richter, H.J.; Wallis, G.B.; Charter, K.H.; Murphy, S.L. Deentrainment and Countercurrent Air–Water Flow in a Model PWR Hot Leg. In *NRC-0193-9*; US Nuclear Regulatory Commission: Rockville, MD, USA, 1978.
53. Ohnuki, A. Experimental Study of Counter-Current Two-Phase Flow in Horizontal Tube Connected to Inclined Riser. *J. Nucl. Sci. Technol.* **1986**, *23*, 219–232. [CrossRef]
54. Weiss, P.A.; Hertlein, R.J. UPTF Test Results: First Three Separate Effect Tests. *Nucl. Eng. Des.* **1988**, *108*, 249–263. [CrossRef]
55. Mayinger, F.; Weiss, P.; Wolfert, K. Two-Phase Flow Phenomena in Full-Scale Reactor Geometry. *Nucl. Eng. Des.* **1993**, *145*, 47–61. [CrossRef]
56. Glaeser, H.; Karwat, H. The Contribution of UPTF Experiments to Resolve Some Scale-up Uncertainties in Countercurrent Two Phase Flow. *Nucl. Eng. Des.* **1993**, *145*, 63–84. [CrossRef]
57. Geffraye, G.; Bazin, P.; Pichon, P.; Bengaouer, A. CCFL in Hot Legs and Steam Generators and Its Prediction with the CATHARE Code. In Proceedings of the 7th International Meeting on Nuclear Reactor Thermal Hydraulics NURETH-7, New York, NY, USA, 10–15 September 1995; pp. 815–826.
58. Chun, M.H.; No, H.C.; Kang, S.K.; Chu, I.C. Countercurrent Flow Limitation in a Horizontal Pipe Connected to an Inclined Riser. *Trans. Am. Nucl. Soc.* **1999**, *81*, 340–341.
59. Navarro, M.A. Countercurrent Flow Limitation in a Horizontal Tube Connected to an Inclined Riser. *Heat Transf. Eng.* **2006**, *27*, 2–8. [CrossRef]
60. Valle'e, C.; Deendarlianto; Beyer, M.; Lucas, D.; Carl, H. Air/Water Counter-Current Flow Experiments in a Model of the Hot Leg of a Pressurized Water Reactor. In Proceedings of the 16th International Conference on Nuclear Engineering, Orlando, FL, USA, 11–15 May 2008; pp. 807–816.
61. Vallée, C.; Seidel, T.; Lucas, D.; Tomiyama, A.; Murase, M. Comparison of Countercurrent Flow Limitation Experiments Performed in Two Different Models of the Hot Leg of a Pressurized Water Reactor with Rectangular Cross Section. *J. Eng. Gas Turbines Power* **2011**, *133*, 052917. [CrossRef]
62. Vallée, C.; Lucas, D.; Tomiyama, A.; Murase, M. Experimental Investigation of Stratified Two-Phase Flows in the Hot Leg of a PWR for CFD Validation. *VGB PowerTech* **2012**, *92*, 40–46.
63. Vallée, C.; Seidel, T.; Lucas, D.; Beyer, M.; Prasser, H.M.; Pietruske, H.; Schütz, P.; Carl, H. Counter-Current Flow Limitation in a Model of the Hot Leg of a PWR—Comparison between Air/Water and Steam/Water Experiments. *Nucl. Eng. Des.* **2012**, *245*, 113–124. [CrossRef]
64. Montoya, G.A.; Deendarlianto; Lucas, D.; Höhne, T.; Vallée, C. Image-Processing-Based Study of the Interfacial Behavior of the Countercurrent Gas-Liquid Two-Phase Flow in a Hot Leg of a PWR. *Sci. Technol. Nucl. Install.* **2012**, *2012*, 209542. [CrossRef]
65. Lucas, D.; Beyer, M.; Pietruske, H.; Szalinski, L. Counter-Current Flow Limitation for Air-Water and Steam-Water Flows in a PWR Hot Leg Geometry. *Nucl. Eng. Des.* **2017**, *323*, 56–67. [CrossRef]
66. Minami, N.; Nishiwaki, D.; Nariai, T.; Tomiyama, A.; Murase, M. Countercurrent Gas-Liquid Flow in a Pwr Hot Leg under Reflux Cooling (i) Air-Water Tests for 1/15-Scale Model of a Pwr Hot Leg. *J. Nucl. Sci. Technol.* **2010**, *47*, 142–148. [CrossRef]
67. Kinoshita, I.; Nriai, T.; Tomiyama, A.; Lucas, D.; Murase, M. Effects of Liquid Properties on CCFL in a Scaled-Down Model of a PWR Hot Leg. *J. Power Energy Syst.* **2011**, *5*, 316–329. [CrossRef]
68. Al Issa, S.; Macian-Juan, R. Experimental Investigation of CCFL in Large Diameter Hot-Leg Geometry. In Proceedings of the 21st International Conference on Nuclear Engineering, Chengdu, China, 2 August 2013.
69. Al Issa, S.; MacIan-Juan, R. Experimental Investigation of Countercurrent Flow Limitation (CCFL) in a Large-Diameter Hot-Leg Geometry: A Detailed Description of CCFL Mechanisms, Flow Patterns and High-Quality HSC Imaging of the Interfacial Structure in a 1/3.9 Scale of PWR Geometry. *Nucl. Eng. Des.* **2014**, *280*, 550–563. [CrossRef]
70. Al Issa, S.; Macián-Juan, R. Image-Processing of Time-Averaged Interface Distributions Representing CCFL Characteristics in a Large Scale Model of a PWR Hot-Leg Pipe Geometry. *Ann. Nucl. Energy* **2017**, *103*, 282–293. [CrossRef]
71. Al Issa, S.; Murase, M.; Tomiyama, A.; Hayashi, K.; Macián-Juan, R. On CCFL at a PWR Hot-Leg Pipe Geometry and Comparison Between Results in COLLIDER 1/4th- and Kobe 1/15th-Scaled Facilities. *Nucl. Sci. Eng.* **2019**, *193*, 147–159. [CrossRef]
72. Badarudin, A.; Indarto; Deendarlianto; Setyawan, A. Characteristics of the Air-Water Counter Current Two-Phase Flow in a 1/30 Scale of Pressurized Water Reactor (PWR): Interfacial Behavior and CCFL Data. *AIP Conf. Proc.* **2016**, *1737*, 040015. [CrossRef]

73. Badarudin, A.; Setyawan, A.; Dinaryanto, O.; Widyatama, A.; Indarto; Deendarlianto. Interfacial Behavior of the Air-Water Counter-Current Two-Phase Flow in a 1/30 Scale-down of Pressurized Water Reactor (PWR) Hot Leg. *Ann. Nucl. Energy* **2018**, *116*, 376–387. [CrossRef]
74. Astyanto, A.H.; Pramono, J.A.E.; Catrawedarma, I.G.N.B.; Deendarlianto; Indarto. Statistical Characterization of Liquid Film Fluctuations during Gas-Liquid Two-Phase Counter-Current Flow in a 1/30 Scaled-down Test Facility of a Pressurized Water Reactor (PWR) Hot Leg. *Ann. Nucl. Energy* **2022**, *172*, 109065. [CrossRef]
75. Wongwises, S. Experimental Investigation of Two-Phase Countercurrent Flow Limitation in a Bend between Horizontal and Inclined Pipes. *Exp. Therm. Fluid Sci.* **1994**, *8*, 245–259. [CrossRef]
76. Wongwises, S. Flooding in a Horizontal Pipe with Bend—Brief Communication. *Int. J. Multiph. Flow* **1996**, *22*, 195–201. [CrossRef]
77. Wongwises, S. Two-Phase Countercurrent Flow in a Model of a Pressurized Water Reactor Hot Leg. *Nucl. Eng. Des.* **1996**, *166*, 121–133. [CrossRef]
78. Kim, H.T.; No, H.C. Assessment of RELAP5/MOD3.2.2γ against Flooding Database in Horizontal-to-Inclined Pipes. *Ann. Nucl. Energy* **2002**, *29*, 835–850. [CrossRef]
79. D'Auria, F.; Galassi, G.M. Scaling in Nuclear Reactor System Thermal-Hydraulics. *Nucl. Eng. Des.* **2010**, *240*, 3267–3293. [CrossRef]
80. Glaeser, H.; Rohatgi, U.S. Scaling Ability of the Counter-Current Flow Limitation (CCFL) Correlations for Application to Reactor Thermal Hydraulics. *Nucl. Eng. Des.* **2019**, *354*, 110226. [CrossRef]
81. Takeuchi, K.; Young, M.Y.; Gagnon, A.F. Flooding in the Pressurizer Surge Line of AP600 Plant and Analyses of APEX Data. *Nucl. Eng. Des.* **1999**, *192*, 45–58. [CrossRef]
82. Futatsugi, T.; Yanagi, C.; Murase, M.; Hosokawa, S.; Tomiyama, A. Countercurrent Air-Water Flow in a Scale-down Model of a Pressurizer Surge Line. *Sci. Technol. Nucl. Install.* **2012**, *2012*, 174838. [CrossRef]
83. Yu, J.; Zhang, D.; Shi, L.; Tian, W.; Su, G.H.; Qiu, S.Z. Experimental Investigation of Entrainment Effect on the Countercurrent Flow in the Hot Leg and Pressurizer Surge Line Assembly of Third-Generation Passive Nuclear Reactors. *Nucl. Eng. Des.* **2018**, *335*, 326–338. [CrossRef]
84. Yu, J.; Zhang, D.; Shi, L.; Wang, Z.; Tian, W.; Su, G.H.; Qiu, S.Z. Experimental Research on the Characteristics of Steam-Water Counter-Current Flow in the Pressurizer Surge Line Assembly. *Exp. Therm. Fluid Sci.* **2018**, *96*, 180–191. [CrossRef]
85. Takaki, T.; Murase, M.; Nishida, K.; Torige, T.; Tomiyama, A. Countercurrent Flow Limitation at a Square Top End of Vertical Pipes and in a Pressurizer Surge Line. *Nucl. Eng. Des.* **2020**, *363*, 110624. [CrossRef]
86. Yamamoto, Y.; Murase, M.; Tomiyama, A. Countercurrent Flow Limitation in a Pressurizer Surge Line. *Nucl. Eng. Des.* **2018**, *326*, 175–182. [CrossRef]
87. Kroleswki, S.M. Flooding Limits in a Simulated Nuclear Reactor Hot Leg. Master's Thesis, MIT, Cambridge, MA, USA, 1980.
88. Kawaji, M.; Thomson, L.A.; Krishnan, V.S. Countercurrent Flooding in an Elbow between a Vertical Pipe and a Downwardly Inclined Pipe. In Proceedings of the 4th International Topical Meeting on Nuclear Reactor Thermal-Hydraulics (NURETH-4), Karlsruhe, Germany, 10–13 October 1989; pp. 20–27.
89. Kawaji, M.; Thomson, L.A.; Krishnan, V.S. Countercurrent Flooding in Vertical-to-Inclined Pipes. *Exp. Heat Transf.* **1991**, *4*, 95–110. [CrossRef]
90. Ghiaasiaan, S.M.; Turk, R.E.; Abdel-Khalik, S.I. Countercurrent Flow Limitation in Inclined Channels with Bends. *Nucl. Eng. Des.* **1994**, *152*, 379–388. [CrossRef]
91. Ghiaasiaan, S.M.; Wu, X.; Sadowski, D.L.; Abdel-Khalik, S.I. Hydrodynamic Characteristics of Counter-Current Two-Phase Flow in Vertical and Inclined Channels: Effects of Liquid Properties. *Int. J. Multiph. Flow* **1997**, *23*, 1063–1083. [CrossRef]
92. Ohnuki, A.; Adachi, H.; Murao, Y. Scale Effects on Countercurrent Gas-Liquid Flow in a Horizontal Tube Connected to an Inclined Riser. *Nucl. Eng. Des.* **1988**, *107*, 283–294. [CrossRef]
93. Al Issa, S. A New Correlation for CCFL at Full Scale PWR Excluding the Hutze Effect in UPTF Data. *Nucl. Eng. Des.* **2021**, *383*, 111402. [CrossRef]
94. Bankoff, S.G.; Tankin, R.S.; Yuen, M.C. Countercurrent Flow of Air/Water and Steam/Water through a Horizontal Perforated Plate. *Int. J. Heat Mass Transf.* **1981**, *24*, 1381–1395. [CrossRef]
95. Celata, G.P.; Cumo, M.; Setaro, T. Flooding in Inclined Pipes with Obstructions. *Exp. Therm. Fluid Sci.* **1992**, *5*, 18–25. [CrossRef]
96. Kawaji, M.; Lotocki, P.A.; Krishnan, V.S. Countercurrent Flooding in Pipes Containing Multiple Elbows and an Orifice. *JSMEA Int. J.* **1993**, *36*, 397–403. [CrossRef]
97. Teyssedou, A.; Önder, E.N.; Tye, P. Air-Water Counter-Current Slug Flow Data in Vertical-to-Horizontal Pipes Containing Orifice Type Obstructions. *Int. J. Multiph. Flow* **2005**, *31*, 771–792. [CrossRef]
98. Wang, M.J.; Mayinger, F. Simulation and Analysis of Thermal-Hydraulic Phenomena in a PWR Hot Leg Related to SBLOCA. *Nucl. Eng. Des.* **1995**, *155*, 643–652. [CrossRef]
99. Tye, P.F. Counter-Current Flow and Flooding in Vertical and Horizontal Tubes with and without Obstructions. Ph.D. Thesis, Ecole Polytechnique, Montreal, QC, Canada, 1998.
100. Deendarlianto, D.; Höhne, T.; Lucas, D.; Vallée, C.; Zabala, G.A.M. CFD Studies on the Phenomena around Counter-Current Flow Limitations of Gas/Liquid Two-Phase Flow in a Model of a PWR Hot Leg. *Nucl. Eng. Des.* **2011**, *241*, 5138–5148. [CrossRef]
101. Kinoshita, I.; Murase, M.; Utanohara, Y.; Lucas, D.; Vallée, C.; Tomiyama, A. Effects of Shape and Size on Countercurrent Flow Limitation in Flow Channels Simulating a PWR Hot Leg. *Nucl. Technol.* **2014**, *187*, 44–56. [CrossRef]

102. Murase, M.; Utanohara, Y.; Kinoshita, I.; Minami, N.; Tomiyama, A. Numerical Calculations on Countercurrent Air-Water Flow in Small-Scale Models of a PWR Hot Leg Using a VOF Model. In Proceedings of the 17th International Conference on Nuclear Engineering, Brussels, Belgium, 12–16 July 2009; pp. 141–148.
103. Minami, N.; Murase, M.; Tomiyama, A. Countercurrent Gas-Liquid Flow in a PWR Hot Leg under Reflux Cooling (II) Numerical Simulation of 1/15-Scale Air-Water Tests. *J. Nucl. Sci. Technol.* **2010**, *47*, 149–155. [CrossRef]
104. Kinoshita, I.; Murase, M.; Utanohara, Y.; Minami, N.; Tomiy, A. Numerical Simulation of Countercurrent Gas-Liquid Flow in a PWR Hot Leg under Reflux Cooling. *J. Nucl. Sci. Technol.* **2010**, *47*, 963–972. [CrossRef]
105. Murase, M.; Tomiyama, A.; Kinoshita, I.; Utanohara, Y.; Yanagi, C.; Takata, T.; Yamaguchi, A. VOF Calculations of Countercurrent Gas-Liquid Flow in a PWR Hot Leg. *Sci. Technol. Nucl. Install.* **2012**, *2012*. [CrossRef]
106. Murase, M.; Utanohara, Y.; Kinoshita, I.; Yanagi, C.; Takata, T.; Yamaguchi, A.; Tomiyama, A. VOF Simulations of Countercurrent Gas-Liquid Flow in a PWR Hot Leg. *J. Comput. Multiph. Flows* **2012**, *4*, 375–386. [CrossRef]
107. Murase, M.; Tomiyama, A.; Lucas, D.; Kinoshita, I.; Utanohara, Y.; Yanagi, C. Correlation for Countercurrent Flow Limitation in a PWR Hot Leg. *J. Nucl. Sci. Technol.* **2012**, *49*, 398–407. [CrossRef]
108. Utanohara, Y.; Kinoshita, I.; Murase, M.; Minami, N.; Nariai, T.; Tomiyama, A. Numerical Simulation Using CFD Software of Countercurrent Gas-Liquid Flow in a PWR Hot Leg under Reflux Condensation. *Nucl. Eng. Des.* **2011**, *241*, 1643–1655. [CrossRef]
109. Utanohara, Y.; Kinoshita, I.; Murase, M.; Lucas, D.; Vallée, C.; Tomiyama, A. Numerical Simulations for Steam-Water CCFL Tests Using the 1/3 Scale Rectangular Channel Simulating a PWR Hot Leg. *Nucl. Eng. Des.* **2012**, *249*, 14–23. [CrossRef]
110. Kinoshita, I.; Murase, M.; Tomiyama, A. Numerical Simulation of Size Effects on Countercurrent Flow Limitation in PWR Hot Leg Models. *Sci. Technol. Nucl. Install.* **2012**, *2012*, 907364. [CrossRef]
111. Höhne, T.; Deendarlianto; Lucas, D. Numerical Simulations of Counter-Current Two-Phase Flow Experiments in a PWR Hot Leg Model Using an Interfacial Area Density Model. *Int. J. Heat Fluid Flow* **2011**, *32*, 1047–1056. [CrossRef]
112. Höhne, T. Deendarlianto Numerical Simulations of Counter Current Flow Experiments Using a Morphology Detection Algorithm. *J. Comput. Multiph. Flows* **2012**, *4*, 271–286. [CrossRef]
113. Porombka, P.; Höhne, T. Drag and Turbulence Modelling for Free Surface Flows within the Two-Fluid Euler-Euler Framework. *Chem. Eng. Sci.* **2015**, *134*, 348–359. [CrossRef]
114. Wintterle, T.; Laurien, E. Numerical Simulation of Flow Reversal in Countercurrent Horizontal Stratifeid Flows. In Proceedings of the 21 International Conference on Nuclear Engineering, Nice, France, 22–27 April 2007.
115. Wintterle, T.; Laurien, E.; Stäbler, T.; Meyer, L.; Schulenberg, T. Experimental and Numerical Investigation of Counter-Current Stratified Flows in Horizontal Channels. *Nucl. Eng. Des.* **2008**, *238*, 627–636. [CrossRef]
116. Al Issa, S.; Macian-Juan, R. Experimental Investigation and CFD Validation of Countercurrent Flow Limitation (CCFL) in a Large-Diameter PWR Hot-Leg Geometry. *J. Nucl. Sci. Technol.* **2016**, *53*, 647–655. [CrossRef]
117. Watanabe, T.; Takata, T.; Yamaguchi, A. Numerical Study on Modeling of Liquid Film Flow under Countercurrent Flow Limitation in Volume of Fluid Method. *Nucl. Eng. Des.* **2017**, *313*, 447–457. [CrossRef]
118. Samal, K.; Ghosh, S. Characterization and Prediction of Flow-Conditions in the Hot-Leg of PWR during Loss of Coolant Accident. *Nucl. Eng. Des.* **2020**, *359*, 110446. [CrossRef]
119. Höhne, T.; Vallée, C. Experiments and Numerical Simulations of Horizontal Two-Phase Flow Regimes Using an Interfacial Area Density Model. *J. Comput. Multiph. Flows* **2010**, *2*, 131–143. [CrossRef]
120. Chen, H.D.; Zhang, X.Y. Numerical Simulation of Countercurrent Flow Based on Two-Fluid Model. *Nucl. Eng. Des.* **2017**, *313*, 361–369. [CrossRef]
121. Riva, E.D.; Col, D.D. Numerical Simulation of Churn Flow in a Vertical Pipe. *Chem. Eng. Sci.* **2009**, *64*, 3753–3765. [CrossRef]
122. Tekavcic, M.; Koncar, B.; Kljenak, I. Simulation of Flooding Waves in Vertical Churn Flow. *Nucl. Eng. Des.* **2016**, *299*, 214–224. [CrossRef]
123. Sampaio, P.A.B.; Faccini, J.L.H.; Su, J. Modelling of Stratified Gas-Liquid Two-Phase Flow in Horizontal Circular Pipes. *Int. J. Heat Mass Transf.* **2008**, *51*, 2752–2761. [CrossRef]
124. Vallée, C.; Höhne, T.; Prasser, H.M.; Sühnel, T. Experimental Investigation and CFD Simulation of Horizontal Stratified Two-Phase Flow Phenomena. *Nucl. Eng. Des.* **2008**, *238*, 637–646. [CrossRef]
125. Deendarlianto; Andrianto, M.; Widyaparaga, A.; Dinaryanto, O.; Khasani; Indarto. CFD Studies on the Gas-Liquid Plug Two-Phase Flow in a Horizontal Pipe. *J. Pet. Sci. Eng.* **2016**, *147*, 779–787. [CrossRef]
126. Akhlaghi, M.; Mohammadi, V.; Nouri, N.M.; Taherkhani, M.; Karimi, M. Multi-Fluid VoF Model Assessment to Simulate the Horizontal Air–Water Intermittent Flow. *Chem. Eng. Res. Des.* **2019**, *152*, 48–59. [CrossRef]
127. Zhang, Y.; He, C.; Li, P. Numerical Investigation of Gas-Liquid Two-Phase Flow in Horizontal Pipe with Orifice Plate. *Prog. Nucl. Energy* **2021**, *138*, 103801. [CrossRef]